The Drosophila Fab-7 boundary modulates Abd-B gene activity by guiding an inversion of collinear chromatin organization and alternate promoter use

Laura Moniot-Perron, Benoit Moindrot, Line Manceau, Joanne Edouard, Yan Jaszczyszyn, Pascale Gilardi-Hebenstreit, Céline Hernandez, Sébastien Bloyer, Daan Noordermeer

Cell Reports

Article

The *Drosophila* Fab-7 boundary modulates *Abd-B* gene activity by guiding an inversion of collinear chromatin organization and alternate promoter use

Graphical abstract

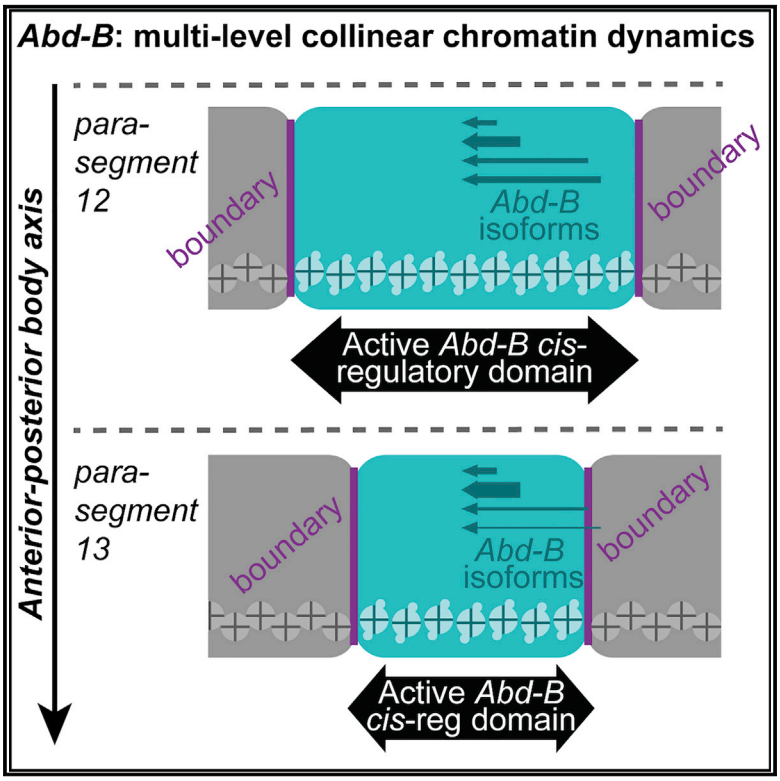

Highlights

- Boundary elements separate domains of 3D genome organization and histone modifications
- Different pairs of boundaries can separate the active *Abd-B cis*-regulatory domain
- *Abd-B* chromatin dynamics follow a non-canonical inversion of collinearity
- Dynamic regulatory hierarchies drive differential *Abd-B* alternative promoter use

Authors

Laura Moniot-Perron, Benoit Moindrot, Line Manceau, ..., Céline Hernandez, Sébastien Bloyer, Daan Noordermeer

Correspondence

sebastien.bloyer@i2bc.paris-saclay.fr (S.B.), daan.noordermeer@i2bc.paris-saclay.fr (D.N.)

In brief

Moniot-Perron et al. determine gene-regulatory hierarchies for the *Abd-B Drosophila Hox* gene. Boundary elements are essential to separate *cis*-regulatory regions, allowing differential 3D chromatin organization and domains of histone modifications. This multilevel organization creates a non-canonical inversion of collinear chromatin dynamics at *Abd-B*, which drives differential alternative promoter use.

Moniot-Perron et al., 2023, Cell Reports *42*, 111967
January 31, 2023
https://doi.org/10.1016/j.celrep.2022.111967

CellPress

Cell Reports

CellPress
OPEN ACCESS

Article

The *Drosophila* Fab-7 boundary modulates *Abd-B* gene activity by guiding an inversion of collinear chromatin organization and alternate promoter use

Laura Moniot-Perron,[1,3] Benoit Moindrot,[1] Line Manceau,[2] Joanne Edouard,[1] Yan Jaszczyszyn,[1] Pascale Gilardi-Hebenstreit,[2] Céline Hernandez,[1] Sébastien Bloyer,[1,*] and Daan Noordermeer[1,4,*]

[1]Université Paris-Saclay, CEA, CNRS, Institute for Integrative Biology of the Cell (I2BC), 91190 Gif-sur-Yvette, France
[2]Université Paris Cité, CNRS, Institut Jacques Monod, 75013 Paris, France
[3]Present address: European Molecular Biology Laboratory (EMBL), Heidelberg 69117, Germany
[4]Lead contact
*Correspondence: sebastien.bloyer@i2bc.paris-saclay.fr (S.B.), daan.noordermeer@i2bc.paris-saclay.fr (D.N.)
https://doi.org/10.1016/j.celrep.2022.111967

SUMMARY

Hox genes encode transcription factors that specify segmental identities along the anteroposterior body axis. These genes are organized in clusters, where their order corresponds to their activity along the body axis, a feature known as collinearity. In *Drosophila*, the BX-C cluster contains the three most posterior *Hox* genes, where their collinear activation incorporates progressive changes in histone modifications, chromatin architecture, and use of boundary elements and *cis*-regulatory regions. To dissect functional hierarchies, we compare chromatin organization in cell lines and larvae, with a focus on the *Abd-B* gene. Our work establishes the importance of the Fab-7 boundary for insulation between 3D domains carrying different histone modifications. Interestingly, we detect a non-canonical inversion of collinear chromatin dynamics at *Abd-B*, with the domain of active histone modifications progressively decreasing in size. This dynamic chromatin organization differentially activates the alternative promoters of the *Abd-B* gene, thereby expanding the possibilities for fine-tuning of transcriptional output.

INTRODUCTION

Hox genes encode crucial developmental regulators that specify segmental identities along the anteroposterior (A-P) body axis in the embryo of bilaterian species. A unique feature of *Hox* genes is that they are organized in clusters, with their genomic position corresponding to their order of expression along the A-P axis.[1] This feature, known as collinearity, was discovered in *Drosophila melanogaster* and was later observed in other bilaterian species, including mammals, as well.[2,3] Because of this evolutionarily conserved structure/function relationship, *Hox* genes have been intensively studied to decipher cluster-wide coordination of gene regulation.[4–7]

In *D. melanogaster*, the eight *Hox* genes are organized in two separate clusters on chromosome 3R: the Antennapedia cluster (ANT-C) and the Bithorax cluster (BX-C). The 350 kb BX-C contains the *Ubx*, *abd-A*, and *Abd-B* genes, which specify the identity of the posterior parasegments 5 to 14 (PS5 to PS14) in the embryo. To drive *Hox* gene expression in the correct PS, the BX-C is subdivided into 10 *cis*-regulatory regions (*abx*/*bx*, *bxd*/*pbx*, and the infra-abdominal segments 2 to 9 [*iab-2* to *iab-9*]). Each *cis*-regulatory region contains cell-type and PS-specific enhancers and is both essential and sufficient to drive the expression of its associated *Hox* gene within a single PS.[8–12]

The collinear activation of the *Hox* genes and their *cis*-regulatory elements has been proposed to rely on a progressive opening of chromatin within the BX-C along the A-P axis. In this "open for business" model, the repressive H3K27me3 histone modification (associated with Polycomb group proteins) at each *cis*-regulatory region is sequentially substituted by the active H3K4me3 mark (associated with Trithorax group proteins).[13–15] Consequently, in the most anterior PS5, *abx*/*bx* is the only *cis*-regulatory region that is marked by H3K4me3, whereas in more posterior PSs, an increasing number of *cis*-regulatory regions are included. This model has been confirmed from embryonic PS4 to PS7, where the repressive H3K27me3 mark is sequentially removed from *abx*/*bx* to *iab-3*.[16] An alternative organization has been detected in the SF4/Sg4 cell lines, though, where activity of the *Abd-B* gene depends on the *iab-7 cis*-regulatory region.[15,17,18] Here, H3K4me3 was present only at *iab-7* to *iab-9*, whereas the more anterior *Ubx* and *abd-A* genes and their *cis*-regulatory regions carried the repressive H3K27me3 mark. In these cells, whose use of the *iab-7 cis*-regulatory region mirrors PS12, the active *cis*-regulatory domain had thus reduced in size. Based on these contrasting observations, it remains to be determined if the "open for business" model expands toward posterior PSs or, instead, if the organization as observed in the SF4/Sg4 cell lines expands to other posterior *iabs*.

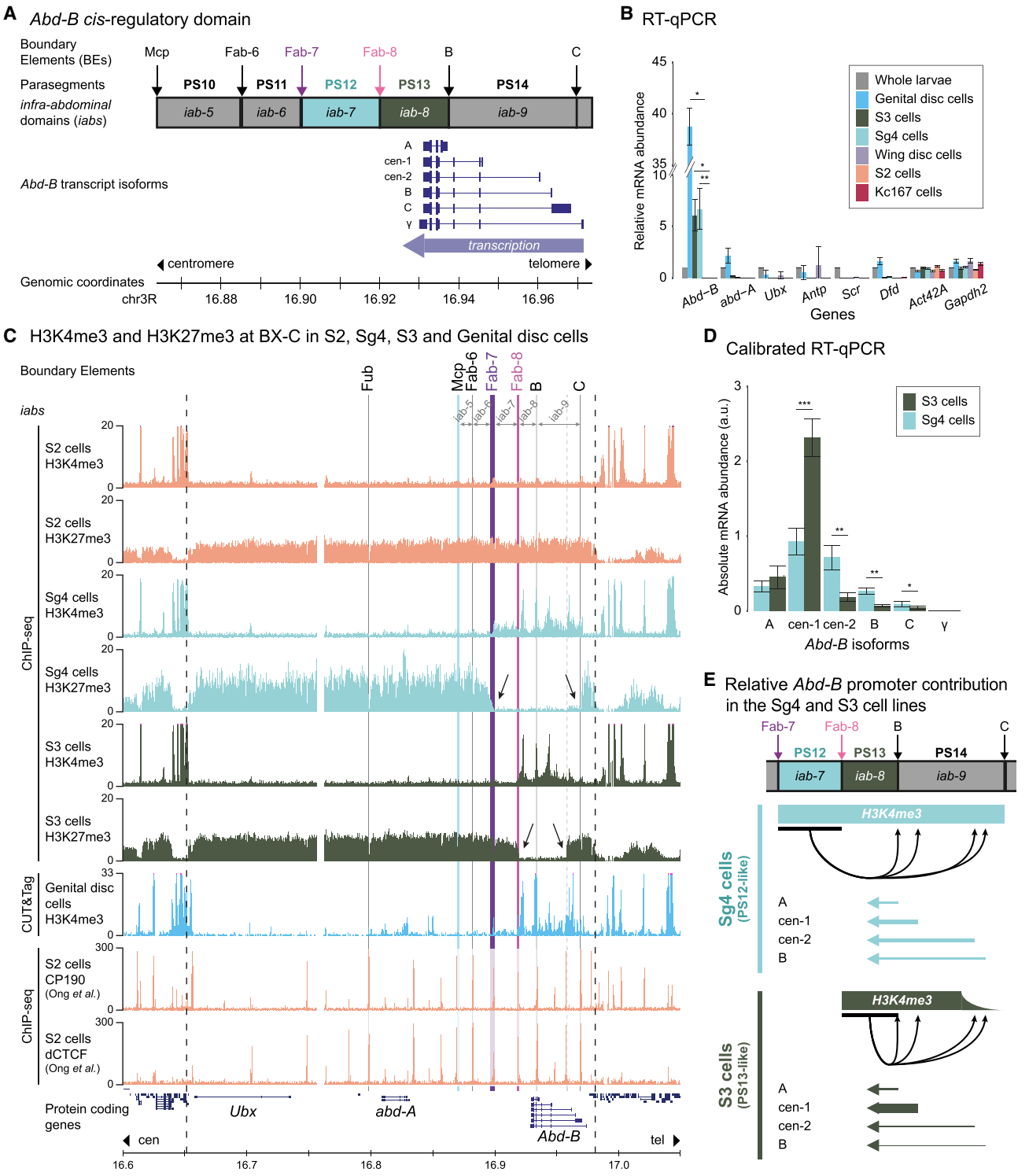

Figure 1. Gene expression and histone modification landscape of the BX-C in cell lines and imaginal disc cells

(A) Overview of the *cis*-regulatory landscape around the *Abd-B* gene and its transcript isoforms. The infra-abdominal domains (*iabs*) and associated embryonic parasegments (PS) are indicated on top, with BEs that separate *iabs* positioned in-between. *iab-7*, active in PS12, is highlighted in blue and *iab-8*, active in PS13, is highlighted in green. Different *Abd-B* transcript isoforms are indicated at the bottom, with the order of transcription visualized with the arrow.

(B) Relative *Hox* gene mRNA amounts in imaginal disc cells and cell lines. The qRT-PCR signal is expressed relative to whole larvae and shown relative to the *Act42A* and *Gapdh2* housekeeping genes. Data are from biological replicates (n = 2). Error bars indicate standard deviation. T test; *p < 0.05, **p < 0.01.

(legend continued on next page)

Genomic regions that carry the same histone modifications adopt a higher-order 3D configuration that is known as a "contact domain," where intradomain interactions are enriched over the surrounding DNA.[19,20] Circular chromosome conformation capture (4C-seq) and Hi-C studies in *Drosophila* larvae and cell lines have confirmed that the repressed BX-C forms a contact domain that matches the distribution of the H3K27me3 mark.[4,19,21] At mammalian *Hox* clusters, the sequential substitution of H3K27me3 by H3K4me3 along the A-P axis coincides with inactive and active contact domains of different size.[22] Contact domain dynamics along the *Drosophila* A-P axis have not been reported, but imaging studies have identified an activity-dependent sequence of association and separation between the *Ubx* and the *abd-A* genes at anterior positions in the embryo.[23,24] In contrast, active *Abd-B* does not appear to reassociate with *Ubx* and *abd-A* at posterior positions. Likewise, comparative Chromosome Conformation Capture (3C) experiments at BX-C in the *Drosophila* S2 and S3 cell lines showed that the active *Abd-B* gene and its associated *cis*-regulatory regions reduced their contacts with the inactive *Ubx* and *abd-A* genes.[25] This different behavior may suggest that contact domains are differentially organized depending on which gene in the BX-C is active.

The restriction of *cis*-regulatory region activity to a single PS depends on the use of boundary elements (BEs) between these regions.[26] For example, deletion of the Fab-7 boundary between *iab-6* and *iab-7* causes an ectopic activation of *iab-7* in PS11, in addition to the normal activity of *iab-6*.[27] Smaller deletions within Fab-7 can have opposing effects in subsets of PS11 cells, though, resulting in silencing of both *iab-6* and *iab-7*.[28] This is likely caused by the bipartite organization of Fab-7, which includes binding sites for insulator proteins and a Polycomb and a Trithorax response element (PRE and TRE).[26,28–30]

How different gene-regulatory layers, including *cis*-regulatory regions, histone modification domains, contact domains, and BEs, functionally intersect to establish cell-type-specific transcriptional programs during development remains a topic of intense interest.[31–34] Taking advantage of the detailed knowledge about the *cis*-regulatory organization of the BX-C, we have dissected hierarchies among its gene-regulatory layers, with a particular focus on the *Abd-B* gene. By combining high-resolution genomics data from larval imaginal discs and cell lines, we found that the function of the Fab-7 BE extended to the insulation between histone modification domains and contact domains. Unexpectedly, in cell lines that represent PS12 and PS13, the organization of histone modification domains and contact domains was inversed, with an active H3K4me3 domain of decreased size at a more posterior position. Combination of precisely calibrated and single-cell transcription analysis revealed that the active *iabs* differentially instructed alternative *Abd-B* promoter use, thereby providing the means for fine-tuning of transcriptional output.

RESULTS

Drosophila imaginal discs and cell lines exhibit similar *Hox* gene activity patterns

The *Abd-B* gene is regulated by a 100 kb *cis*-regulatory domain that consists of five *iabs.* In-between each pair of two *iabs* a BE is located. Transcription of *Abd-B* can be initiated from six alternative promoters that are located in *iab-8*, in *iab-9*, or telomeric from *iab-9* (Figure 1A). Except for the A promoter, current annotations indicate that all transcripts encode the same Abd-B protein isoform (NCBI RefSeq genes, FlyBase Release 6.32; Celniker et al.[35]; and Zavortink et al.[36]). To investigate how BEs, domains of histone modifications, and 3D contact domains converge to regulate the *Abd-B* gene, we first identified cellular models where *Abd-B* is differentially expressed. Using qRT-PCR, we analyzed *Abd-B* and five other *Hox* genes in two imaginal discs from larvae and in four cell lines (Figure 1B). The genital disc is a mixed population of cells from the most posterior PSs in the larvae, whereas wing disc cells originate from a more anterior position.[37]

Compared with whole larvae, *Abd-B* mRNA levels were increased in genital disc cells. Significantly elevated *Abd-B* amounts were detected in the Sg4 and S3 cell lines as well, albeit at lower levels as in the genital disc. No significant activity of *Abd-B* or the other *Hox* genes was detected in the wing disc or the S2 and Kc167 cell lines (Figure 1B). Our analysis thus revealed comparable patterns of *Hox* gene activities in the genital disc and Sg4 and S3 cell lines, which included a shared activity of *Abd-B*. Similarly, the wing disc shared the absence of *Hox* gene activity with the S2 and Kc167 cell lines.

Histone modification domains mirror *Abd-B* promoter activity, yet reveal an inverse collinear distribution

To determine how histone modifications at the *Hox* clusters correlated with gene expression, we performed H3K4me3 and H3K27me3 chromatin immunoprecipitation sequencing (ChIP-seq) experiments in S2, Sg4, and S3 cells, supplemented with H3K4me3 CUT&Tag (Cleavage Under Targets and Tagmentation) in genital discs. At the ANT-C, where no substantial *Hox* gene activity was detected in any of the cell types, repressive H3K27me3 covered the entire domain. Conversely, the H3K4me3 mark was mostly absent, with the exception of minor peaks at certain inactive *Hox* gene promoters (Figure S1A). This contrasted with the BX-C, where cell-type-specific differences in

(C) ChIP-seq data for the H3K4me3 and H3K27me3 histone marks in the S2, Sg4, and S3 cell lines and H3K4me3 CUT&Tag data in genital disc cells. Reanalyzed ChIP-seq data for the CP190 and dCTCF insulator proteins in the S2 cell line are indicated below.[38] The BX-C is demarcated by dashed lines, with known BEs highlighted by vertical bars. Relevant BEs and *iabs* are indicated on top. Arrows indicate the BEs that act as a boundary between the histone modification domains in the different cell lines. Protein coding genes are indicated at the bottom.

(D) Calibrated qRT-PCR data of alternative *Abd-B* promoter activity in S3 and Sg4 cells. Data are normalized to an exon shared between all isoforms and to an external plasmid containing all isoform-specific amplicons. Data are from biological replicates (n = 2). Error bars indicate standard deviation. T test; $*p < 0.05$, $**p < 0.01$, $***p < 0.001$.

(E) Scheme of *Abd-B* promoter contribution relative to the extent of the H3K4me3 histone modification domain in the Sg4 cell line (PS12-like cells, blue) and the S3 cell line (PS13-like cells, green). On top, the positions of BEs and *iabs* are indicated, with the extent of the H3K4me3 domains indicated below. The thickness of the arrow tails reflects the relative contribution of each promoter.

histone modifications could be detected. In S2 cells, the inactive BX-C was fully covered by H3K27me3, with no peaks of H3K4me3 at any of the *Hox* gene promoters (Figures 1C, S1B, and S1C). In genital discs and the Sg4 and S3 cell lines, the active *Abd-B* gene and its surrounding *cis*-regulatory domain were enriched for H3K4me3. Interestingly, the distributions of H3K4me3 and H3K27me3 over the active *Abd-B cis*-regulatory domain were not identical. In Sg4 cells, the entire region spanning *iab-7* to *iab-9* was devoid of H3K27me3 and enriched for H3K4me3, with the Fab-7 and C BEs acting as boundaries (Figure 1C, arrows, and Figures S1B and S1D). In contrast, in S3 cells the H3K27me3 mark was present at *iab-7* and the telomeric part of *iab-9.* Conversely, H3K4me3 was absent from *iab-7* and strongly reduced at the telomeric part of *iab-9* in these cells. In these cells, the Fab-8 BE acted as a centromeric boundary, whereas the telomeric boundary was not associated with an annotated BE (Figure 1C, arrows, and Figures S1B and S1D). To investigate if an unidentified BE existed within *iab-9*, we reanalyzed ChIP-seq data for the CP190 and dCTCF insulator proteins in the S2 cell line and cells of embryonic and larval origin.[38–40] This analysis revealed a strongly occupied site in-between the B and the C BEs that exactly overlapped the boundary in S3 cells (Figure 1C, dashed lines, and Figure S1D).

Previous genetic studies have assigned the activity of BEs and *iabs* to individual PSs (summarized in Kyrchanova et al.[26]). Based on the use of BEs and *iabs* in the Sg4 and S3 cell lines, we concluded that the Sg4 cell line mimicked PS12, whereas the S3 cell line mimicked PS13. H3K4me3 CUT&Tag data in genital disc cells suggested a more mixed organization, with robust H3K4me3 signal detected in *iab-8* and *iab-9* and a minor enrichment at *iab-7*. Notably, in Sg4 and S3 cells, the inactive *Ubx* and *abd-A* genes and the *Abd-B*-associated *iab-5* and *iab-6* were fully covered by H3K27me3 (Figure 1C). Activity of *Abd-B* in these cells was therefore associated with an inverse collinear presence of the repressive H3K27me3 mark at the centromeric side of the domain, which differentially included *iab-7* depending on the use of Fab-7 or Fab-8 as the BE.

The peaks of H3K4me3 enrichment overlapped different sets of alternative *Abd-B* promoters, with five of six promoters covered in Sg4 cells (A to C) and only the A and cen-1 promoters robustly marked in S3 cells (Figures 1A, 1C, and S1E). We therefore wondered if these cell types displayed a different preference for *Abd-B* promoter use. Calibrated qRT-PCR, normalized to a shared *Abd-B* sequence, was used to quantify the relative contribution of each *Abd-B* promoter (Figure 1D). Comparison between the Sg4 and the S3 cell lines revealed that the cen-1 promoter was used significantly more in S3 cells, whereas the cen-2 and B promoters contributed significantly more in Sg4 cells (Figure 1D). The combined outputs from these promoters are mostly similar between these two cell types, though (Figure 1B). Alternative *Abd-B* promoter activity thus mirrored the presence of H3K4me3 peaks in these cell lines, yet achieved a similar combined transcriptional output (Figure 1E).

The inactive BX-C is organized into two 3D contact domains

To assess the link between domains of histone modifications and 3D chromatin architecture at the *Hox* gene clusters, we used genome-wide Hi-C and viewpoint-specific 4C-seq (an assay that has been extensively used to study *Hox* gene architecture[21,22,41–43]). We first focused on the 3D organization of the inactive clusters, which are covered by the repressive H3K27me3 mark. By combining reanalyzed Hi-C data[44] with newly generated 4C-seq data in S2 cells, we observed that the BX-C and ANT-C restricted most of their interactions within their H3K27me3-marked domains (Figures 2A, S2A, and S2B). The inactive *Hox* clusters were therefore organized into repressed 3D contact domains approximately 300–400 kb in size.[19,20] Calling of domain boundaries using Hi-C data from S2 cells confirmed the overlap with the H3K27me3 histone modification domain, but revealed intradomain boundaries as well: the inactive ANT-C is divided into three subdomains and the BX-C into two subdomains (Figures 2A and S2A). The boundary within the BX-C is the Fub BE, which separates the *Ubx* and *abd*-A *cis*-regulatory domains.[45] Consequently, the inactive *abd-A* and *Abd-B cis*-regulatory domains co-occupy the same contact domain.

Next, we used 4C-seq to address if the same contact domains were present at the inactive ANT-C and BX-C in larval wing discs and the Kc167 cell line. For the analyzed viewpoints, we found interactions highly similar to those in S2 cells, confirming that the inactive *Hox* clusters had adopted a similar 3D contact domain organization (Figures 2B and S2C–S2E).

Active *Abd-B* dissociates from the repressed BX-C contact domains in Sg4 cells

To determine 3D chromatin organization of the *Hox* clusters in cells where *Abd-B* is active, we performed Hi-C and 4C-seq in the Sg4 cell line. Contact domains at the repressed ANT-C in Sg4 cells were comparable to the previously established organization in S2 cells, confirming that the chromatin architecture of this inactive cluster was not drastically reorganized (Figures S2A, S3A, and S3B). In contrast, the 3D organization of the BX-C was markedly different between Sg4 and S2 cells. Our Hi-C analysis revealed that the BX-C in Sg4 cells was organized into three subdomains, with each *Hox* gene occupying its own domain (Figure 3A). Whereas the boundary between the repressed *Ubx* and *abd-A* genes remained at the Fub BE, a new boundary had appeared that coincided with the Fab-7 BE element. 4C-seq confirmed this observation, which was particularly visible upon comparison between *Abd-B* promoter interactions in the Sg4 and S2 cell lines (Figure 3A, yellow shading). In Sg4 cells, the Fab-7 BE acted as the boundary between the *Abd-B* H3K4me3 domain and the H3K27me3 domain consisting of *iab-5*, *iab-6*, and the *abd-A cis*-regulatory domains. The active *Abd-B* domain, bordered by the Fab-7 and C BEs and comprising *iab-7* to *iab-9*, therefore, was organized as an active contact domain that was physically dissociated from the repressed *abd-A* contact domain.

The active *Abd-B* contact domain is bordered by different BEs in different cell types

Next, we wondered if the same contact domain organization was present in the S3 cell line and in larval genital discs, where the *Abd-B* gene is active but associated with H3K4me3 domains of different sizes (Figures 1B and 1C). For the analyzed 4C-seq viewpoints at the ANT-C, which remained in an inactive state in

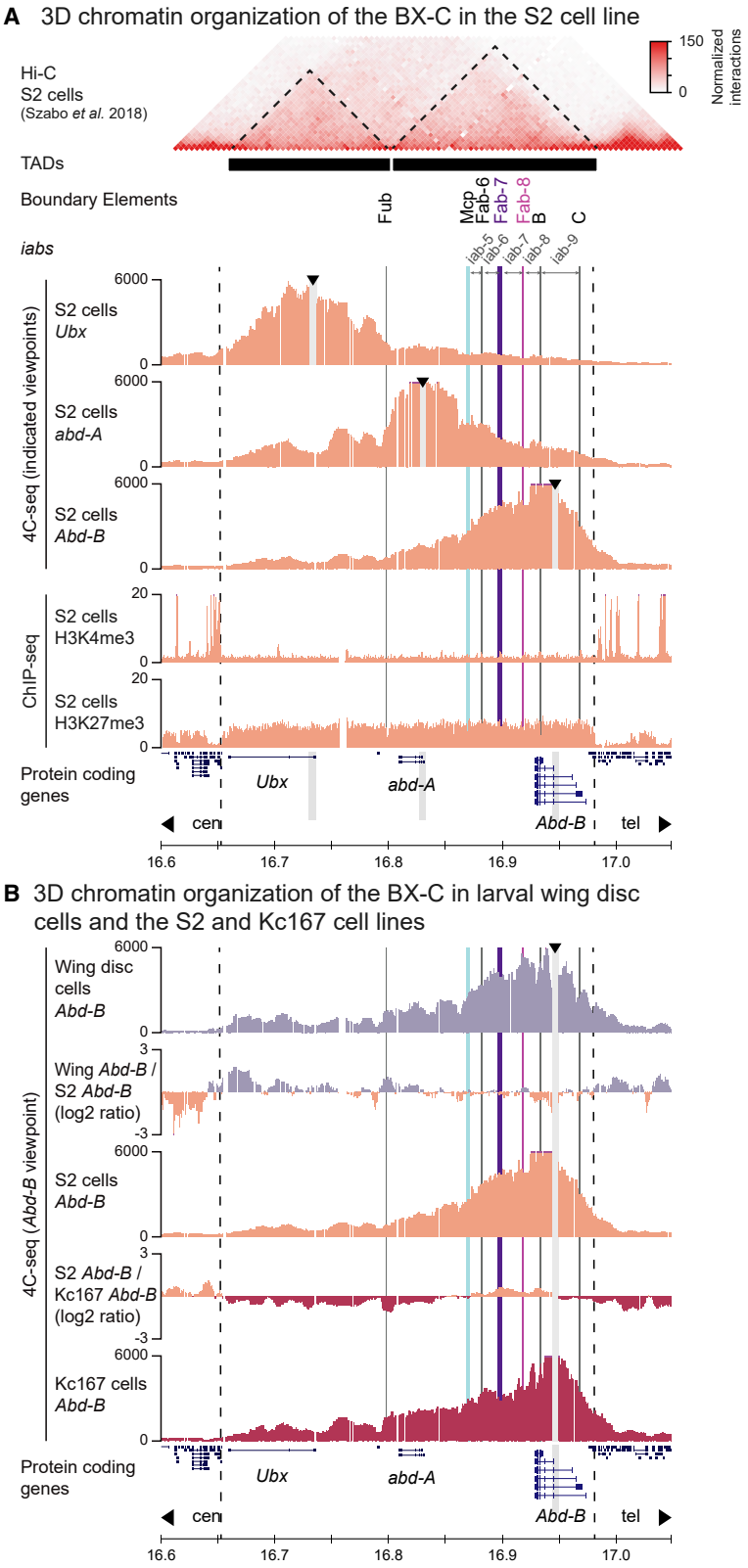

Figure 2. 3D chromatin organization of the repressed BX-C

(A) Hi-C (top), 4C-seq (middle), and ChIP-seq (bottom) data in the S2 cell line. Hi-C data were reanalyzed from Szabo et al.,[44] with identified subdomains indicated as black bars. 4C-seq data for viewpoints in the promoters of the *Ubx*, *abd-A*, and *Abd-B* (cen-1) genes are indicated in-between. H3K4me3 and H3K27 ChIP-seq data are indicated below. Arrowheads indicate the positions of viewpoints. Protein-coding genes are indicated at the bottom. Further annotation is as in Figure 1C.

(B) 4C-seq data in wing disc cells and the S2 and Kc167 cell lines for the *Abd-B* cen-1 promoter viewpoint. In-between, the log2 ratio of interactions is shown. Protein-coding genes are indicated at the bottom.

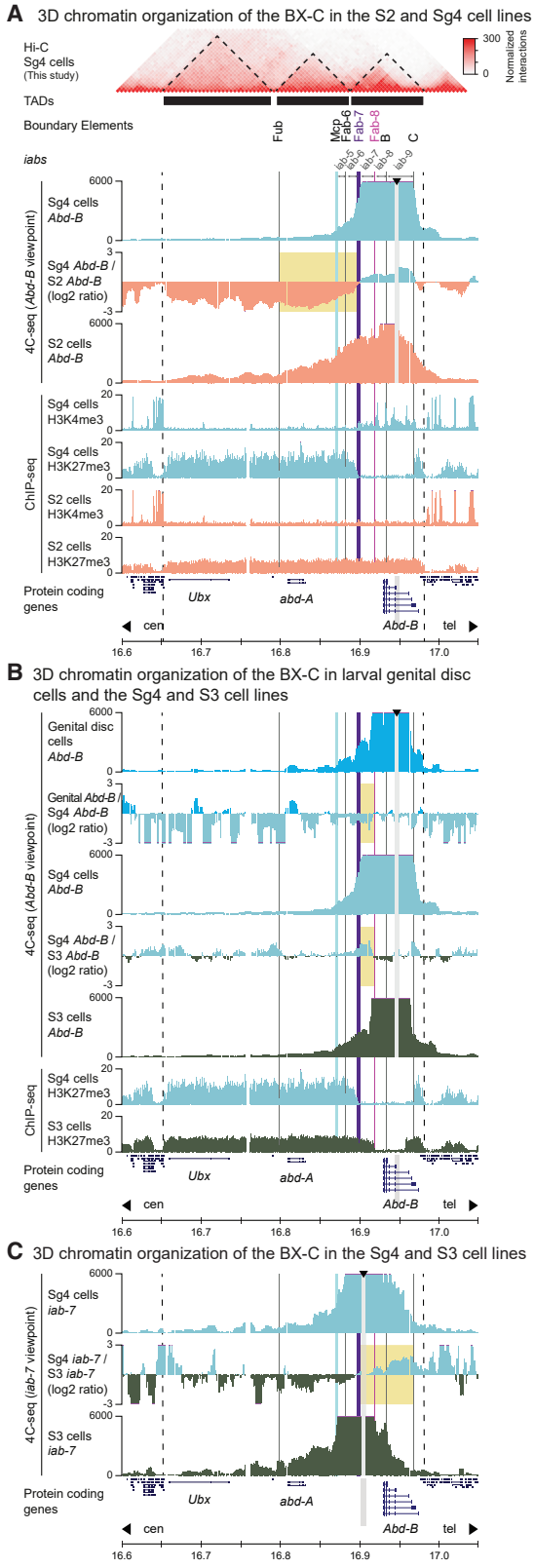

Figure 3. 3D chromatin organization of the BX-C in cell types where *Abd-B* is active

(A) Hi-C (top) and 4C-seq (middle) and ChIP-seq (bottom) data in the Sg4 cell line. Subdomains as identified by Hi-C are indicated as black bars. The 4C-seq data for the *Abd-B* cen-1 promoter viewpoint in S2 (*Abd-B* inactive) and Sg4 cell lines are shown with the log2 ratio of interactions indicated in-between. The yellow rectangle highlights the domain of reduced interactions in Sg4 cells whose right border coincides with the Fab-7 BE. H3K4me3 and H3K27 ChIP-seq data in the S2 and Sg4 cell lines are indicated below. Arrowhead indicates the position of the viewpoint. Protein-coding genes are indicated at the bottom. Further annotation is as in Figure 1C.

(B) 4C-seq data in genital disc cells and the Sg4 and S3 lines for the *Abd-B* cen-1 promoter viewpoint. In-between, the log2 ratio of interactions is shown. Yellow rectangles highlight the domains of increased interactions in Sg4 cells that cover *iab-7*. Protein-coding genes are indicated at the bottom.

(C) 4C-seq data in the Sg4 and S3 cell lines for the *iab-7* viewpoint. In-between, the log2 ratio of interactions is shown. The yellow rectangle highlights the domain of increased interactions in Sg4 cells that covers *iab-9*. Protein-coding genes are indicated at the bottom.

these cells, we could not detect a major reorganization of contacts (Figures S3A, S3C, and S3D). Comparison of interactions at the BX-C in these cells confirmed the spatial separation of *Abd-B* from the inactive part of the cluster, but also revealed noticeable differences in 3D contact domain boundaries (Figure 3B). In Sg4 cells, a steep drop in interactions coincided with the Fab-7 BE, whereas a similar drop in S3 cells coincided with the Fab-8 BE. As a result, the *Abd-B* cen-1 promoter viewpoint contacted the *iab-7* considerably more in the Sg4 cell line compared with S3 cells (Figure 3B; yellow shading). Conversely, the inactive *Ubx* and *abd-A* promoters contacted *iab-7* more in S3 cells (Figure S3E). This observation was further confirmed using a viewpoint at *iab-7* itself, which associated more with the active *iab-8* and *iab-9* in Sg4 cells and with the centromeric inactive part of the BX-C in S3 cells (Figure 3C, yellow shading). The use of different BEs in the different cell lines thus mirrored the boundaries of the different H3K4me3 domains (Figure 1C), and the association of *iab-7* with the active or inactive contact domain directly coincided with the presence of the H3K4me3 or H3K27me3 histone modification.

A similar difference for the *Abd-B* viewpoint was observed comparing genital discs to the Sg4 cell line, although the heterogeneous nature of the genital disc provided less discrete patterns of interactions. In the genital disc, a steep drop in interactions coincided with the Fab-8 BE (like in S3 cells), yet a minor drop at the Fab-7 BE was observed as well (like in Sg4 cells). Both BEs thus appear to contribute to the separation between the active and the inactive contact domain, with *iab-7* differentially associating with either domain (Figure 3B, yellow shading).

These observations confirmed the direct overlap between histone modification domains and 3D contact domains and identified BEs as the DNA elements that provide cell-type-specific separation between the 3D histone modification domains of varying size.

Absence of the Fab-7 BE reduces overall *Abd-B* activity in genital discs

To assess the importance of BE function in separating histone modification and contact domains in a developmental context, we analyzed an existing *Drosophila* mutant line in which the

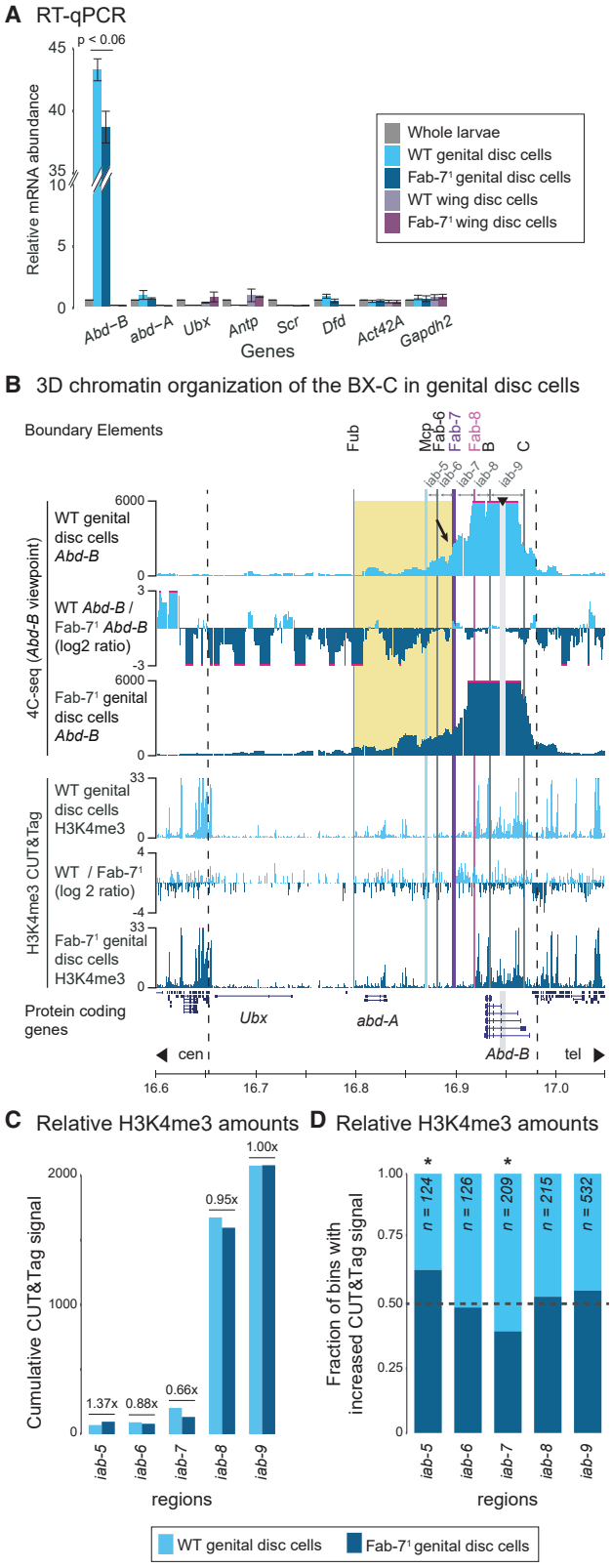

Figure 4. *Hox* gene expression and 3D chromatin organization in WT and Fab-7[1] deletion larval imaginal disc cells

(A) Relative *Hox* gene mRNA amounts in WT and Fab-7[1] deletion wing and genital disc cells (blue). qRT-PCR signal is normalized to the *Act42A* and *Gapdh2* housekeeping genes and relative to WT whole larvae. Data are from biological replicates (n = 2). Error bars indicate standard deviation. T test.

(B) 4C-seq (top) and H3K4me3 CUT&Tag (bottom) data in WT and Fab-7[1] deletion genital disc cells. 4C-seq data are shown for the *Abd-B* cen-1 promoter viewpoint, with the log2 ratio of interactions indicated in-between. The abrupt drop in interactions at the Fab-7 BE in WT cells is indicated by the arrow, and the region with increased interactions over the *abd-A* gene in Fab-7[1] deletion cells is highlighted with the yellow rectangle. The log2 ratio of CUT&Tag signal (50 bp bins) is indicated in-between the tracks. Protein-coding genes are indicated at the bottom. Further annotation is as in Figure 1C.

(C) Cumulative H3K4me3 CUT&Tag signal in the indicated *iabs*. The ratio in signal is indicated above the bars, with values >1 indicating a gain of domain-wide signal in Fab-7[1] deletion cells and values <1 indicating a loss of domain-wide signal.

(D) Fraction of H3K4me3 CUT&Tag bins (50 bp windows, normalized signal) with increased signal in WT or Fab-7[1] deletion cells. G test of independence; *p < 0.05.

Fab-7 element is absent.[27] In this Fab-7[1] strain, the deletion of a 4.3 kb DNA fragment that encompasses both its BE and its PRE function causes the ectopic activation of *iab-7* in the more anterior abdominal segments of the adult fly.[27,46,47] To determine how the Fab-7 BE affected global *Hox* gene expression in larvae, we performed qRT-PCR in genital and wing disc cells from the wild-type (WT) and homozygous Fab-7[1] strains. The larval genital disc is thought to encompass the most posterior PSs (from PS13), whereas our results suggested a contribution from PS12 as well (Figure 3B; Kyrchanova et al.,[26] and Sanchez and Guerrero[48]). Upon removal of the Fab-7 BE, all *Hox* genes remained inactive in wing disc cells, yet in genital disc cells, we observed a 10% reduction in *Abd-B* mRNA abundance (Figure 4A). The Fab-7 BE, which borders *iab-7* that is active in PS12, therefore, positively contributed to overall *Abd-B* mRNA abundance in the genital disc.

Absence of Fab-7 reorganizes contact domains and histone modification domains

Next, we used 4C-seq to determine if the absence of the Fab-7 BE had a noticeable effect on 3D contact domain structure. In wing disc cells, where *Abd-B* is repressed, our 4C-seq viewpoints revealed no obvious differences between WT and deletion cells (Figure S4A). In genital disc cells, considerable differences were observed, though. Whereas the steep drop in interactions at the Fab-8 BE remained in the absence of Fab-7 (pink line), the smaller drop that was observed at the WT Fab-7 BE (purple line) had disappeared (Figure 4B). Moreover, in the absence of the Fab-7 BE, the interactions of the *Abd-B* viewpoint were increased over the entire BX-C, with particularly more signal now detected in the *abd-A cis*-regulatory domain (Figure 4B, yellow shading). Conversely, the inactive *Ubx* and *abd-A* viewpoints increased their contacts with the *Abd-B* regulatory domain, which was particularly prominent at *iab-7* (Figure S4B). Based on the patterns that we observed in the Sg4 and S3 cell lines, we envision that the separation between the active and the inactive contact domains at the Fab-7 BE had been lost in the subset of PS12 cells within the heterogeneous genital disc (Figure 3B,

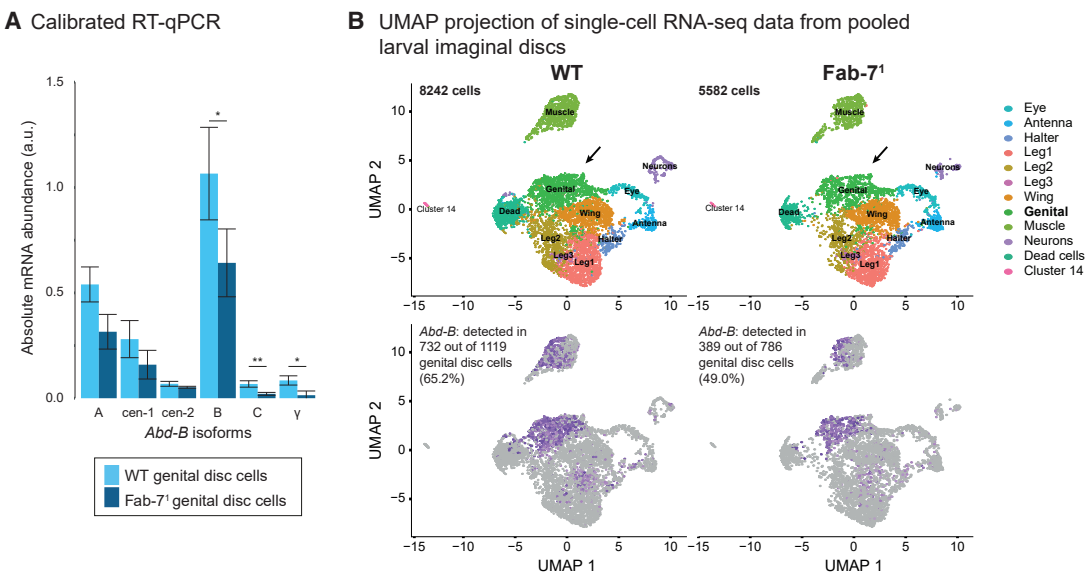

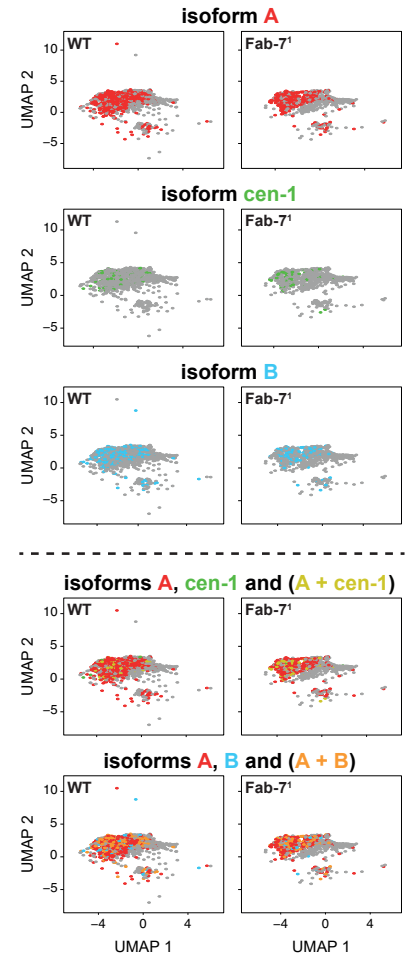

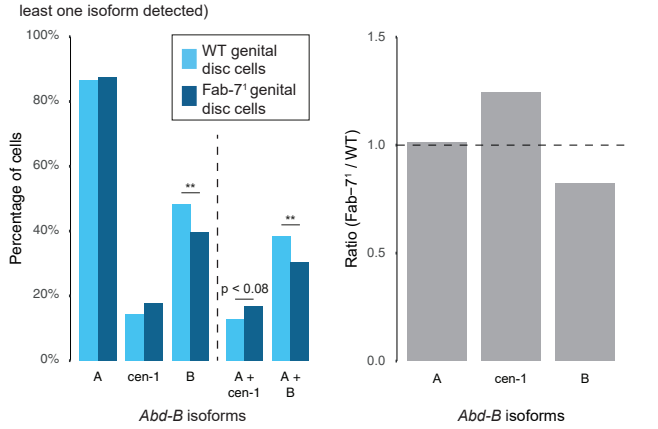

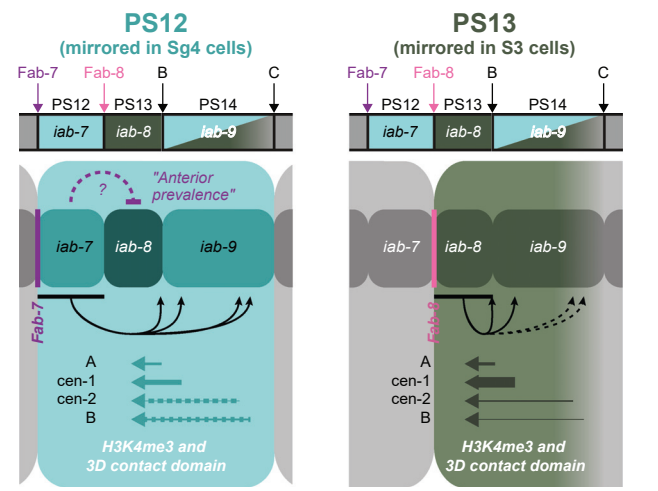

(legend on next page)

drop in interactions at the Fab-7 and Fab-8 BEs). The loss of separation between the active and the inactive contact domains, as observed by 4C-seq, created an organization with similarities to the S2 cell line (Figures 2A and 3A). The increased association with the repressive contact domain in the PS12 subset of genital disc cells may thus explain the observed reduction in global *Abd-B* mRNA levels (Figure 4A).

To determine if the increased association with the inactive contact domain had an influence on the H3K4me3 histone modification domain, we generated H3K4me3 and H3K27me3 CUT&Tag data in Fab-7 deletion genital discs (Figure 4B, bottom tracks, and Figures S4C and S4D). Visual inspection of H3K27me3 revealed a consistent enrichment over the entire *Abd-B* regulatory domain, indicating that WT genital discs also included a considerable fraction of cells where *Abd-B* was repressed (Figure S4D). Comparison of H3K4me3 distribution revealed a significant 1.5-fold reduction in this active mark within *iab-7* in cells where Fab-7 was absent. In contrast, the mark was significantly increased within *iab-5*, although the overall signal remained low. Within the mixed cell population of the genital disc, no significant difference was detected at *iab-8* and *iab-9*, where the majority of *Abd-B* promoters are localized (Figures 4C and 4D). The reduced H3K4me3 levels at the *iab-7* regulatory domain therefore emerged as the most apparent link with the globally decreased *Abd-B* activity. As both Fab-7 and *iab-7* activities are associated with PS12, we hypothesize that the loss of H3K4me3 in this PS was directly correlated with the reduced contacts with the upstream active contact domain.

Absence of Fab-7 reorganizes *Abd-B* promoter choice in genital disc cells

Next we wondered if the observed reduction in H3K4me3 at *iab-7* in the absence of the Fab-7 BE could be associated with a different choice of *Abd-B* promoters, similar to the Sg4 and S3 cell lines (Figure 1D). We first assessed *Abd-B* promoter choice using calibrated qRT-PCR in WT and Fab-7^1 genital disc cells (Figure 5A). Confirming our previous observation that *Abd-B* activity was reduced in the absence of Fab-7, we noticed that mRNA for most *Abd-B* isoforms was less abundant, with additional relative differences between promoters visible as well (Figures 4A and 5A). Of note, both the minor reduction for the cen-2 promoter and the unexpectedly large reduction for the B promoter indicated different activities of these promoters in the PS12 cells of the genital discs compared with the Sg4 cell line, which mimics the same PS (Figures 1D and 5A). The differential use of promoters extended to the embryonic stage, where the most abundant *Abd-B* isoforms were reduced to varying degrees as well (Figure S5A).

The pan-cellular nature of our qRT-PCR-based analysis in the heterogeneous genital disc precluded a distinction between a global reduction of *Abd-B* expression and reduced numbers of *Abd-B*-expressing cells. To overcome this limitation, we performed single-cell RNA sequencing (RNA-seq) analysis on pools of larval imaginal discs (see STAR Methods for details). Promoter choice was determined by sequencing the 5′ end of the mRNA molecules in the single-cell RNA-seq libraries. After quality filtering, we obtained data from 8,242 WT cells and 5,582 Fab-7 deletion cells (Figure 5B, top). Although fewer Fab-7^1 cells were recovered, similar numbers of unique mRNA molecules and annotated transcripts were detected in both genotypes, thus confirming comparable data quality (Figures S5B and S5C). Clustering of the combined WT and Fab-7^1 deletion data identified 14 distinct clusters of cells. Based on tissue-specific marker genes, including the *Hox* genes, we traced back the eight dissected imaginal discs and four other cell populations that were inadvertently recovered as well (Figures 5B and S5D). Both genital discs and muscle cells could be traced back to two clusters, which were merged in the downstream analysis. Importantly, all remaining clusters contained a mix of WT and Fab-7^1 deletion cells, confirming that the absence of the Fab-7 BE did not influence cell and cluster identity (Figure 5B). Notably, we could detect mRNA from all other *Hox* genes in small numbers of genital disc cells, showing that the repression of *Hox* genes in the larval genital disc is not complete (Figure S5D and Table S1). Similar observations were made in wing disc cells and in single-cell RNA-seq analysis of the Sg4 and S2 cell lines, where *abd-A* mRNA was detected in a subset of Sg4 cells (Figure S5E and Table S1).

Abd-B transcripts, originating from any promoter, were almost exclusively detected in the genital disc cluster, in both the WT and the Fab-7^1 deletion cells (Figure 5B). We therefore restricted the remainder of our analysis to this cluster, which comprised 1,119 WT and 786 Fab-7^1 cells. We detected *Abd-B* transcripts

Figure 5. *Abd-B* promoter activity in WT and Fab-7^1 deletion imaginal disc cells

(A) Calibrated qRT-PCR data of alternative *Abd-B* promoters in WT and Fab-7 deletion genital disc cells. Data are normalized to an exon shared between all isoforms and to an external plasmid containing all isoform-specific amplificons. Data are from biological replicates (n = 2). Error bars indicate standard deviation. T test; *p < 0.05, **p < 0.01.

(B) UMAP (Uniform Manifold Approximation and Projection) of combined single-cell RNA-seq data from pools of WT and Fab-7 deletion imaginal discs. Top: identified clusters, comprising the eight different discs and four other clusters (with data separated for WT [left] and Fab-7 deletion [right] cells). Arrows indicate the merged genital disc cluster. Bottom: presence of *Abd-B* mRNA (purple) within the pools of imaginal disc cells.

(C) UMAP of genital disc cells for the indicated *Abd-B* promoters (top) and pairs of promoters (bottom). Color coding as indicated in the headers.

(D) Percentage of cells where mRNA from the indicated promoters or pairs of promoters is detected (percentages in the population of cells where at least one *Abd-B* isoform is detected). G test of independence; **p < 0.01.

(E) Ratio of detected *Abd-B* mRNA (Fab-7^1 deletion/WT genital disc cells) originating from the A, cen-1, and B promoters. Values >1 indicate more positive cells in Fab-7^1 deletion cells and values <1 indicate less positive cells.

(F) Scheme of chromatin organization and *Abd-B* promoter use in cells from PS12 (blue) and PS13 (green). The large spheres indicate the H3K4me3 and 3D contact domains, with *iabs* positioned within. Black arrows indicate transcriptionally activating influence of the *iabs* on the *Abd-B* promoters. The purple dashed line indicates a hypothetical anterior prevalence in PS12 cells whereby *iab-7* maintains *iab-8* in an inactive state. The thickness of the arrow tails indicates the relative contribution of each promoter, with the cen-2 and B isoforms in PS12 indicated as dotted lines due to different activity in cell lines and genital discs. On top the positions of BEs and *iabs* are indicated.

in 65% of WT cells, yet this was reduced to 49% of Fab-7 deletion cells (Figure 5B and Table S1; despite similar quality metrics). Our detection by qRT-PCR of reduced *Abd-B* expression levels in the Fab-7[1] genital disc, associated with the repression of *iab-7* in PS12 cells, could therefore be (partially) explained by fewer cells where *Abd-B* was robustly expressed (Figures 4A and 5B).

Next, we assessed *Abd-B* transcripts originating from different promoters in cells where at least one *Abd-B* isoform was detected. mRNA originating from the A, cen-1, and B promoters was present in the largest numbers of individual cells, which was in line with our calibrated qRT-PCR result (Figures 5A and S5F). By focusing on these three promoters, we identified differences in the response to Fab-7 removal and associated *iab-7* repression in PS12 cells (Figures 5C–5E). Whereas the relative number of cells containing mRNA from the A promoter remained similar, the number of cells that were positive for the cen-1 and B promoters showed an opposite pattern. Cells carrying mRNA from the cen-1 promoter were relatively more abundant upon deletion of the Fab-7 BE, whereas relatively more WT cells carried mRNA from the B promoter (Figures 5D and 5E). This observation was further strengthened by limiting the analysis to cells where mRNA from multiple promoters was detected. Indeed, the combination of mRNA from the A and more centromeric cen-1 promoters was enriched upon Fab-7 deletion, and the combination of the A and more telomeric B promoters was enriched in WT cells (Figures 5D and 5E). In the absence of the Fab-7 BE and its associated reduction of H3K4me3 at *iab-7*, therefore, both the number of *Abd-B*-expressing cells was reduced and the relative contribution of *Abd-B* promoters became reorganized. mRNA originating from the cen-1 promoter, located at a centromeric position in *iab-9* and more active in the PS13-mimicking S3 cells, became relatively more abundant. Conversely, mRNA from the more telomeric B promoter, more active in PS12-mimicking Sg4 cells where *iab-7* acts as a *cis*-regulatory region, had a reduced presence. The capacity of *iab-7* to differentially activate promoters was further confirmed by analysis of the *iab-8* transcript, a long non-coding RNA (lncRNA) that has been implicated in the repression of the *abd-A* gene.[49] mRNA from this lncRNA was detected in significantly fewer deletion cells, with a similar reduction compared with the B promoter of *Abd-B* (Figure S5G). Taken together, our single-cell RNA-seq analysis therefore confirmed that the Fab-7 deletion influenced promoter activity in *iab-8* and *iab-9* at two separate levels. First, we detected fewer cells that contributed to *Abd-B* activity in the genital discs, which we interpret as a global absence or strong reduction of activity in PS12 cells. Second, the varying reductions for the different *Abd-B* isoforms and the *iab-8* lncRNA confirmed that cells from PS12 carried a different cocktail of transcript isoforms compared with cells that originated from other PSs (Figure 5F). These data therefore provide further support for our finding in cell lines that the different BEs and associated *iabs* at the BX-C regulatory domain differentially instruct alternative promoters in *iab-8* and *iab-9*.

DISCUSSION

In this study we determined how domains of histone modifications, 3D chromatin organization, and BEs functionally engage at the *Abd-B* regulatory domain. In cells where the BX-C was fully repressed, most of its chromatin interactions overlapped with the presence of the H3K27me3 histone mark, confirming previous observations that repressed histone modifications and contact domains are tightly linked.[24,25] In cells where *Abd-B* was active, the H3K4me3-marked *cis*-regulatory domain was organized into a contact domain that dissociated from the inactive domain. BEs on both sides of the active contact domain acted as boundaries, providing an improved mechanistic explanation for the previous observations that active and inactive genes and domains within the BX-C are physically separated.[23–25] Different BEs acted as boundaries, though, with either the Fab-7 or the Fab-8 BEs separating the histone modification and contact domains on the centromeric side and either the C BE or a previously unidentified BE providing separation on the telomeric side. We argue that these different chromatin organizations represent the organization in PS12 and PS13, which both contribute to the heterogeneous cell population that makes up the genital disc (Figure 5F). Like at mammalian *Hox* gene clusters, active and inactive contact domains of different sizes are therefore present along the *Drosophila* A-P axis.[4,22] Absence of the Fab-7 BE in the genital disc coincided with a loss of H3K4me3 at *iab-7* in a subpopulation of cells, which we hypothesize originated from PS12 where Fab-7 was the active BE. This result establishes the instructive nature of BEs in demarcating histone modification and contact domains. The loss of H3K4me3 over *iab-7* contradicts the outcome in larval PS11, where the absence of Fab-7 causes ectopic activation of *iab-7*.[27] Upon smaller deletions of Fab-7 in PS11, a cross talk between PREs and TREs could induce silencing of *iab-6* and *iab-7* in subsets of cells, though.[28] A PS12-specific cross talk between PREs and TREs in *Fab-6* and *Fab-8* may explain the silencing of *iab-7* in the genital disc.[26]

The chromatin organization of the active domains in PS12 and PS13 covered different numbers of alternative *Abd-B* promoters. As a result, BE use influenced the abundance of *Abd-B* isoforms (Figure 5F). In line with the notion that a single *iab* is responsible for the activation of *Abd-B* in a single PS, we did not detect a large difference in the combined amounts of *Abd-B* transcripts in the Sg4 and S3 cell lines. This raises the question why alternative *Abd-B* promoters are differentially activated by *iab-7* and *iab-8*. Although not fully consistent with the current annotation, previous studies have suggested that the mRNA molecules that originate from the cen-1, cen-2, B, and C promoters encode the same Abd-B protein isoform (Figure 1A; Celniker et al.[35] and Zavortink et al.[36]). Although we cannot rule out that the alternative transcripts have a direct effect on protein abundance (e.g., through different mRNA stability or translation efficiency), another explanation may be that the different promoters provide a means for fine-tuning transcriptional output in the different PSs, either by increasing the total number of transcription initiation events or by buffering against inherently different promoter affinities between enhancers located in *iab-7* and *iab-8*.

According to the ‘‘open for business’’ model for BX-C activation, the H3K27me3 mark should be progressively replaced by the active H3K4me3 mark along the A-P axis.[14,15] Instead, our description of chromatin dynamics in PS12 and PS13 has identified an unexpected inversion of collinear chromatin opening at

the *Abd-B* regulatory domain. Like previous observations in SF4/Sg4 cells, the centromeric part of the BX-C, including the *Abd-B*-regulating *iab-5* and *iab-6*, was covered by the H3K27me3 mark in PS12.[15,17,18] Yet, in S3 cells—representative of the more posterior PS13—this repressive domain had increased in size to include *iab-7* and the telomeric side of *iab-9* as well (Figure 5F). Although we cannot rule out that this inversion of collinearity is unique to larval cells, we consider this unlikely for two reasons. First, the cell lines included in our study are of embryonic origin, and second, our result provides an improved explanation for observations that *Abd-B* does not reassociate with the *Ubx* and *abd-A* genes in the most posterior cell types of the *Drosophila* embryo.[23,24] Intriguingly, in the absence of Fab-7, we and others detected increased interactions of *Abd-B* with the supposedly H3K27me3-marked centromeric part of BX-C (Figure 4B and Mateo et al.[24]). Combined with the considerable reduction in the number of genital disc cells where *Abd-B* mRNA is detected and the supposed restriction of Fab-7 activity in PS12, we hypothesize that the BX-C adopted a repressed chromatin configuration in this cell population, which was reminiscent of the 3D organization in wing disc cells and the S2 and Kc167 cell lines.

The non-canonical inversion of collinearity in the most posterior PSs may relate to the genetic organization of the *Abd-B* *cis*-regulatory domain. Whereas the promoters of the *Ubx* and *abd-A* genes are located in the most centromeric *cis*-regulatory regions for each gene, the promoters of *Abd-B* are located in the telomeric *iab-8* and *iab-9* (Figure 1A). Instead of a sequential addition of *cis*-regulatory regions from the telomeric side, as observed for *Ubx* and *abd-A*, the activation of *Abd-B* by the more centromeric *iabs* may critically depend on the absence of H3K27me3 at the telomeric *iab-8* and *iab-9* as well. PS-specific regulation by enhancers in a single *iab* may subsequently be achieved by two repressive mechanisms that maintain the inactive state of enhancers in the other *iabs* (Figure 5F). First, the more centromeric *iabs*, active in more anterior PSs, are inactivated through the collinear inversion of H3K27me3-mediated repression. This inversed collinear repression is used for *iab-5* and *iab-6* in PS12 and *iab-5* to *iab-7* in PS13. Second, we speculate that the enhancers in the more telomeric *iabs*, which are included in the H3K4me3-marked contact domain, are kept in an inactive state through an ''anterior prevalence'' of the most centromeric active *iab* within the H3K4me3-marked contact domain. In our study, this is particularly relevant for PS12 cells, where the enhancers in *iab-8* are inactive but marked by H3K4me3. Importantly, the mechanistic underpinnings of this anterior prevalence remain to be confirmed. Similarly, it remains to be determined if *Abd-B* activation by *iab-5* and *iab-6* in the more anterior PS10 and PS11, which are not part of the genitalia, incorporate the inversion of collinear chromatin organization and anterior prevalence over enhancers in *iab-6* to *iab-8* as well.

Interestingly, a non-canonical inversion of collinear chromatin dynamics is observed at the mammalian *HoxA* and *HoxD* clusters during development of the mammalian genitalia and digits. In the genitalia and digits, the *Hox* genes that are expressed at anterior positions along the primary A-P axis become marked by repressive H3K27me3 as well.[50,51] In contrast, genes from the ''posterior'' group-9 to group-13 *Hox* genes are active, which are orthologous to *Abd-B* and arose through serial duplications from a shared ancestor.[52] Like in *Drosophila*, the activation of mammalian *Hox* genes in the genitalia and digits requires dynamic contacts with distant enhancers.[50,51] Although the organization of the *cis*-regulatory landscapes has considerably diverged between these evolutionarily distant species, this raises the intriguing possibility that the inversion of collinear chromatin organization involving *Abd-B* class genes is an ancestral feature, possibly associated with the emergence of genitalia. The investigation of the collinear activation of *Abd-B* group genes in the genitalia of other distant bilaterian lineages may confirm if the inversion of collinearity is an evolutionarily conserved feature that has been inherited from a common ancestor.

Limitations of the study

A limitation of our study is that the direct observations of hierarchical differences in gene-regulatory layers were obtained by comparing cell lines. The exact origin of these decades-old cell lines, thought to be of embryonic origin, is difficult to trace back. Moreover, their prolonged *in vitro* cell culture may have introduced changes to gene activity and transcription-regulatory mechanisms. Whereas the use of BEs has remained strictly linked to histone modifications, 3D genome organization, and overall *Abd-B* activity in the cell lines in this study, we cannot exclude that more subtle changes have occurred. The use of larval imaginal discs allowed us to validate a number of observations about hierarchical links between alternative promoters and BEs. At the same time, we noted differences between the cell lines and the larval imaginal discs as well: a strongly elevated activity of the *Abd-B* gene in the genital disc and further differences in the relative contribution of the cen-2 and B promoters. As such, cell lines do not fully recapitulate collinear gene activity in the genital disc. Our validation using a comparison between WT and Fab-7^{1} deletion genital discs was limited to the detection of relatively minor differences, because these cell populations display differences only in the PS12 cells. PS12 cells make up a relatively minor fraction of the genital disc, whereas the contribution of cells originating from PS13 and PS14 should remain unchanged.

For future studies, the use of *in vivo* systems that allow the identification and isolation of specific PSs or cell type is preferred (see, e.g., Bonn et al.[53] and Bowman et al.[16]). Such systems are limited by the numbers of cells that can be recovered, though, and they require the creation of *Drosophila* strains for individual PSs or cell types, making this process laborious and limiting the number of experiments that can be performed. Comprehensive multiscale investigation of complex biological phenomena, like *Hox* gene collinearity, can therefore nonetheless benefit from a combination of *in vivo* and *in vitro* studies.

STAR★METHODS

Detailed methods are provided in the online version of this paper and include the following:

- KEY RESOURCES TABLE
- RESOURCE AVAILABILITY

- Lead contact
- Materials availability
- Data and code availability
- EXPERIMENTAL MODEL AND SUBJECT DETAILS
  - Fly strains
  - Cell lines
- METHODS DETAILS
  - RT-qPCR
  - Calibrated RT-qPCR for absolute quantification of Abd-B isoforms
  - ChIP-seq and ChIP-qPCR
  - CUT&Tag
  - 4C-seq
  - Hi-C
  - Single-cell RNA-seq
- QUANTIFICATION AND STATISTICAL ANALYSIS

SUPPLEMENTAL INFORMATION

Supplemental information can be found online at https://doi.org/10.1016/j.celrep.2022.111967.

ACKNOWLEDGMENTS

We thank Sylvina Bouleau, Emilie Brasset, Fabienne Malagnac, and the members of the Noordermeer lab for useful discussion. We thank Denis Duboule, Maria Cristina Gambetta, and Elissa Lei for comments on the manuscript. We are grateful to François Karch, Jacques Montagne, Vanessa Ribes, and Matthieu Sanial for sharing of reagents and materials. We thank the I2BC High Throughput Sequencing Platform for sequencing experiments and single-cell sequencing library preparation. Work in the Noordermeer lab is supported by the Agence Nationale de la Recherche (ANR-14-ACHN-0009-01, ANR-16-TERC-0027-01, ANR-17-CE12-0001-02, ANR-18-CE12-0022-02, and ANR-21-CE12-0034-01), PlanCancer (19CS145-00), and the Fondation Bettencourt Schueller. L.M.-P. was supported by thesis grants from the Fondation pour la Recherche Médicale (FDT202012010470) and the Université Paris-Saclay (Ecole Doctorale Structure et Dynamique des Systèmes Vivants). L.M. received thesis funding from the Institut Jacques Monod. The funders had no influence on the design of the project or the decision to publish.

AUTHOR CONTRIBUTIONS

Conceptualization, S.B. and D.N.; methodology, L.M.-P., B.M., S.B., and D.N.; formal analysis, L.M.-P., B.M., C.H., and D.N.; investigation, L.M.-P., B.M., L. M., J.E., Y.J., and P.G.-H.; writing – original draft, L.M.-P., S.B., and D.N.; writing – review & editing, L.M.-P., B.M., S.B., and D.N.; supervision, S.B. and D.N.

DECLARATION OF INTERESTS

The authors declare no competing interests.

INCLUSION AND DIVERSITY

We support inclusive, diverse, and equitable conduct of research. One or more of the authors of this paper self-identifies as an underrepresented ethnic minority in their field of research or within their geographical location. One or more of the authors of this paper self-identifies as a member of the LGBTQIA+ community. One or more of the authors of this paper self-identifies as a gender minority in their field of research.

Received: April 26, 2022
Revised: October 9, 2022
Accepted: December 20, 2022

REFERENCES

1. McGinnis, W., and Krumlauf, R. (1992). Homeobox genes and axial patterning. Cell *68*, 283–302.
2. Lewis, E.B. (1978). A gene complex controlling segmentation in Drosophila. Nature *276*, 565–570.
3. Duboule, D., and Dollé, P. (1989). The structural and functional organization of the murine HOX gene family resembles that of Drosophila homeotic genes. EMBO J. *8*, 1497–1505.
4. Noordermeer, D., and Duboule, D. (2013). Chromatin architectures and Hox gene collinearity. Curr. Top. Dev. Biol. *104*, 113–148. https://doi.org/10.1016/B978-0-12-416027-9.00004-8.
5. Hajirnis, N., and Mishra, R.K. (2021). Homeotic genes: clustering, modularity, and diversity. Front. Cell Dev. Biol. *9*, 718308. https://doi.org/10.3389/fcell.2021.718308.
6. Duboule, D. (2022). The (unusual) heuristic value of Hox gene clusters; a matter of time? Dev. Biol. *484*, 75–87. https://doi.org/10.1016/j.ydbio.2022.02.007.
7. Morata, G., and Lawrence, P. (2022). An exciting period of Drosophila developmental biology: of imaginal discs, clones, compartments, parasegments and homeotic genes. Dev. Biol. *484*, 12–21. https://doi.org/10.1016/j.ydbio.2022.01.008.
8. Simon, J., Peifer, M., Bender, W., and O'Connor, M. (1990). Regulatory elements of the bithorax complex that control expression along the anterior-posterior axis. EMBO J. *9*, 3945–3956.
9. Busturia, A., and Bienz, M. (1993). Silencers in abdominal-B, a homeotic Drosophila gene. EMBO J. *12*, 1415–1425.
10. Pirrotta, V. (1995). Chromatin complexes regulating gene expression in Drosophila. Curr. Opin. Genet. Dev. *5*, 466–472. https://doi.org/10.1016/0959-437x(95)90050-q.
11. Mihaly, J., Barges, S., Sipos, L., Maeda, R., Cléard, F., Hogga, I., Bender, W., Gyurkovics, H., and Karch, F. (2006). Dissecting the regulatory landscape of the Abd-B gene of the bithorax complex. Development *133*, 2983–2993. https://doi.org/10.1242/dev.02451.
12. Iampietro, C., Gummalla, M., Mutero, A., Karch, F., and Maeda, R.K. (2010). Initiator elements function to determine the activity state of BX-C enhancers. PLoS Genet. *6*, e1001260. https://doi.org/10.1371/journal.pgen.1001260.
13. Schuettengruber, B., Chourrout, D., Vervoort, M., Leblanc, B., and Cavalli, G. (2007). Genome regulation by polycomb and trithorax proteins. Cell *128*, 735–745.
14. Maeda, R.K., and Karch, F. (2010). Cis-regulation in the Drosophila bithorax complex. Adv. Exp. Med. Biol. *689*, 17–40.
15. Maeda, R.K., and Karch, F. (2015). The open for business model of the bithorax complex in Drosophila. Chromosoma *124*, 293–307. https://doi.org/10.1007/s00412-015-0522-0.
16. Bowman, S.K., Deaton, A.M., Domingues, H., Wang, P.I., Sadreyev, R.I., Kingston, R.E., and Bender, W. (2014). H3K27 modifications define segmental regulatory domains in the Drosophila bithorax complex. Elife *3*, e02833. https://doi.org/10.7554/eLife.02833.
17. Schwartz, Y.B., Kahn, T.G., Nix, D.A., Li, X.Y., Bourgon, R., Biggin, M., and Pirrotta, V. (2006). Genome-wide analysis of Polycomb targets in Drosophila melanogaster. Nat. Genet. *38*, 700–705. https://doi.org/10.1038/ng1817.
18. Beisel, C., Buness, A., Roustan-Espinosa, I.M., Koch, B., Schmitt, S., Haas, S.A., Hild, M., Katsuyama, T., and Paro, R. (2007). Comparing active and repressed expression states of genes controlled by the Polycomb/Trithorax group proteins. Proc. Natl. Acad. Sci. USA *104*, 16615–16620. https://doi.org/10.1073/pnas.0701538104.
19. Sexton, T., Yaffe, E., Kenigsberg, E., Bantignies, F., Leblanc, B., Hoichman, M., Parrinello, H., Tanay, A., and Cavalli, G. (2012). Three-dimensional folding and functional organization principles of the Drosophila genome. Cell *148*, 458–472. https://doi.org/10.1016/j.cell.2012.01.010.

20. Rao, S.S.P., Huntley, M.H., Durand, N.C., Stamenova, E.K., Bochkov, I.D., Robinson, J.T., Sanborn, A.L., Machol, I., Omer, A.D., Lander, E.S., and Aiden, E.L. (2014). A 3D map of the human genome at kilobase resolution reveals principles of chromatin looping. Cell *159*, 1665–1680. https://doi.org/10.1016/j.cell.2014.11.021.

21. Bantignies, F., Roure, V., Comet, I., Leblanc, B., Schuettengruber, B., Bonnet, J., Tixier, V., Mas, A., and Cavalli, G. (2011). Polycomb-dependent regulatory contacts between distant Hox loci in Drosophila. Cell *144*, 214–226. https://doi.org/10.1016/j.cell.2010.12.026.

22. Noordermeer, D., Leleu, M., Splinter, E., Rougemont, J., De Laat, W., and Duboule, D. (2011). The dynamic architecture of Hox gene clusters. Science *334*, 222–225. https://doi.org/10.1126/science.1207194.

23. Cheutin, T., and Cavalli, G. (2018). Loss of PRC1 induces higher-order opening of Hox loci independently of transcription during Drosophila embryogenesis. Nat. Commun. *9*, 3898. https://doi.org/10.1038/s41467-018-05945-4.

24. Mateo, L.J., Murphy, S.E., Hafner, A., Cinquini, I.S., Walker, C.A., and Boettiger, A.N. (2019). Visualizing DNA folding and RNA in embryos at single-cell resolution. Nature *568*, 49–54. https://doi.org/10.1038/s41586-019-1035-4.

25. Lanzuolo, C., Roure, V., Dekker, J., Bantignies, F., and Orlando, V. (2007). Polycomb response elements mediate the formation of chromosome higher-order structures in the bithorax complex. Nat. Cell Biol. *9*, 1167–1174. https://doi.org/10.1038/ncb1637.

26. Kyrchanova, O., Mogila, V., Wolle, D., Magbanua, J.P., White, R., Georgiev, P., and Schedl, P. (2015). The boundary paradox in the Bithorax complex. Mech. Dev. *138*, 122–132. https://doi.org/10.1016/j.mod.2015.07.002.

27. Gyurkovics, H., Gausz, J., Kummer, J., and Karch, F. (1990). A new homeotic mutation in the Drosophila bithorax complex removes a boundary separating two domains of regulation. EMBO J. *9*, 2579–2585.

28. Mihaly, J., Hogga, I., Gausz, J., Gyurkovics, H., and Karch, F. (1997). In situ dissection of the Fab-7 region of the bithorax complex into a chromatin domain boundary and a Polycomb-response element. Development *124*, 1809–1820. https://doi.org/10.1242/dev.124.9.1809.

29. Cavalli, G., and Paro, R. (1998). The Drosophila Fab-7 chromosomal element conveys epigenetic inheritance during mitosis and meiosis. Cell *93*, 505–518. https://doi.org/10.1016/s0092-8674(00)81181-2.

30. Özdemir, I., and Gambetta, M.C. (2019). The role of insulation in patterning gene expression. Genes *10*, 767. https://doi.org/10.3390/genes10100767.

31. de Laat, W., and Duboule, D. (2013). Topology of mammalian developmental enhancers and their regulatory landscapes. Nature *502*, 499–506. https://doi.org/10.1038/nature12753.

32. Sexton, T., and Cavalli, G. (2015). The role of chromosome domains in shaping the functional genome. Cell *160*, 1049–1059. https://doi.org/10.1016/j.cell.2015.02.040.

33. Rowley, M.J., and Corces, V.G. (2018). Organizational principles of 3D genome architecture. Nat. Rev. Genet. *19*, 789–800. https://doi.org/10.1038/s41576-018-0060-8.

34. Glaser, J., and Mundlos, S. (2022). 3D or not 3D: shaping the genome during development. Cold Spring Harb. Perspect. Biol. *14*, a040188. https://doi.org/10.1101/cshperspect.a040188.

35. Celniker, S.E., Keelan, D.J., and Lewis, E.B. (1989). The molecular genetics of the bithorax complex of Drosophila: characterization of the products of the Abdominal-B domain. Genes Dev. *3*, 1424–1436. https://doi.org/10.1101/gad.3.9.1424.

36. Zavortink, M., and Sakonju, S. (1989). The morphogenetic and regulatory functions of the Drosophila Abdominal-B gene are encoded in overlapping RNAs transcribed from separate promoters. Genes Dev. *3*, 1969–1981. https://doi.org/10.1101/gad.3.12a.1969.

37. Casares, F., Sánchez, L., Guerrero, I., and Sánchez-Herrero, E. (1997). The genital disc of Drosophila melanogaster, I. Segmental and compartmental organization. Dev. Genes Evol. *207*, 216–228. https://doi.org/10.1007/s004270050110.

38. Ong, C.T., Van Bortle, K., Ramos, E., and Corces, V.G. (2013). Poly(ADP-ribosyl)ation regulates insulator function and intrachromosomal interactions in Drosophila. Cell *155*, 148–159. https://doi.org/10.1016/j.cell.2013.08.052.

39. Kaushal, A., Dorier, J., Wang, B., Mohana, G., Taschner, M., Cousin, P., Waridel, P., Iseli, C., Semenova, A., Restrepo, S., et al. (2022). Essential role of Cp190 in physical and regulatory boundary formation. Sci. Adv. *8*, eabl8834. https://doi.org/10.1126/sciadv.abl8834.

40. Kaushal, A., Mohana, G., Dorier, J., Özdemir, I., Omer, A., Cousin, P., Semenova, A., Taschner, M., Dergai, O., Marzetta, F., et al. (2021). CTCF loss has limited effects on global genome architecture in Drosophila despite critical regulatory functions. Nat. Commun. *12*, 1011. https://doi.org/10.1038/s41467-021-21366-2.

41. Ghavi-Helm, Y., Klein, F.A., Pakozdi, T., Ciglar, L., Noordermeer, D., Huber, W., and Furlong, E.E.M. (2014). Enhancer loops appear stable during development and are associated with paused polymerase. Nature *512*, 96–100. https://doi.org/10.1038/nature13417.

42. Narendra, V., Rocha, P.P., An, D., Raviram, R., Skok, J.A., Mazzoni, E.O., and Reinberg, D. (2015). CTCF establishes discrete functional chromatin domains at the Hox clusters during differentiation. Science *347*, 1017–1021. https://doi.org/10.1126/science.1262088.

43. Pinglay, S., Bulajić, M., Rahe, D.P., Huang, E., Brosh, R., Mamrak, N.E., King, B.R., German, S., Cadley, J.A., Rieber, L., et al. (2022). Synthetic regulatory reconstitution reveals principles of mammalian Hox cluster regulation. Science *377*, eabk2820. https://doi.org/10.1126/science.abk2820.

44. Szabo, Q., Jost, D., Chang, J.M., Cattoni, D.I., Papadopoulos, G.L., Bonev, B., Sexton, T., Gurgo, J., Jacquier, C., Nollmann, M., et al. (2018). TADs are 3D structural units of higher-order chromosome organization in Drosophila. Sci. Adv. *4*, eaar8082. https://doi.org/10.1126/sciadv.aar8082.

45. Bender, W., and Lucas, M. (2013). The border between the ultrabithorax and abdominal-A regulatory domains in the Drosophila bithorax complex. Genetics *193*, 1135–1147. https://doi.org/10.1534/genetics.112.146340.

46. Karch, F., Galloni, M., Sipos, L., Gausz, J., Gyurkovics, H., and Schedl, P. (1994). Mcp and Fab-7: molecular analysis of putative boundaries of cis-regulatory domains in the bithorax complex of Drosophila melanogaster. Nucleic Acids Res. *22*, 3138–3146. https://doi.org/10.1093/nar/22.15.3138.

47. Singh, N.P., and Mishra, R.K. (2015). Specific combinations of boundary element and Polycomb response element are required for the regulation of the Hox genes in Drosophila melanogaster. Mech. Dev. *138*, 141–150. https://doi.org/10.1016/j.mod.2015.07.016.

48. Sánchez, L., and Guerrero, I. (2001). The development of the Drosophila genital disc. Bioessays *23*, 698–707. https://doi.org/10.1002/bies.1099.

49. Gummalla, M., Maeda, R.K., Castro Alvarez, J.J., Gyurkovics, H., Singari, S., Edwards, K.A., Karch, F., and Bender, W. (2012). abd-A regulation by the iab-8 noncoding RNA. PLoS Genet. *8*, e1002720. https://doi.org/10.1371/journal.pgen.1002720.

50. Montavon, T., Soshnikova, N., Mascrez, B., Joye, E., Thevenet, L., Splinter, E., de Laat, W., Spitz, F., and Duboule, D. (2011). A regulatory archipelago controls Hox genes transcription in digits. Cell *147*, 1132–1145. https://doi.org/10.1016/j.cell.2011.10.023.

51. Lonfat, N., Montavon, T., Darbellay, F., Gitto, S., and Duboule, D. (2014). Convergent evolution of complex regulatory landscapes and pleiotropy at Hox loci. Science *346*, 1004–1006. https://doi.org/10.1126/science.1257493.

52. Izpisúa-Belmonte, J.C., Falkenstein, H., Dollé, P., Renucci, A., and Duboule, D. (1991). Murine genes related to the Drosophila AbdB homeotic genes are sequentially expressed during development of the posterior part of the body. EMBO J. *10*, 2279–2289.

53. Bonn, S., Zinzen, R.P., Girardot, C., Gustafson, E.H., Perez-Gonzalez, A., Delhomme, N., Ghavi-Helm, Y., Wilczyński, B., Riddell, A., and Furlong, E.E.M. (2012). Tissue-specific analysis of chromatin state identifies

temporal signatures of enhancer activity during embryonic development. Nat. Genet. *44*, 148–156. https://doi.org/10.1038/ng.1064.

54. Miranda, M., Noordermeer, D., and Moindrot, B. (2022). Detection of allele-specific 3D chromatin interactions using high-resolution in-nucleus 4C-seq. Methods Mol. Biol. *2532*, 15–33. https://doi.org/10.1007/978-1-0716-2497-5_2.
55. Langmead, B., and Salzberg, S.L. (2012). Fast gapped-read alignment with Bowtie 2. Nat. Methods *9*, 357–359. https://doi.org/10.1038/nmeth.1923.
56. Danecek, P., Bonfield, J.K., Liddle, J., Marshall, J., Ohan, V., Pollard, M.O., Whitwham, A., Keane, T., McCarthy, S.A., Davies, R.M., and Li, H. (2021). Twelve years of SAMtools and BCFtools. GigaScience *10*, giab008. https://doi.org/10.1093/gigascience/giab008.
57. Ramírez, F., Ryan, D.P., Grüning, B., Bhardwaj, V., Kilpert, F., Richter, A.S., Heyne, S., Dündar, F., and Manke, T. (2016). deepTools2: a next generation web server for deep-sequencing data analysis. Nucleic Acids Res. *44*, W160–W165. https://doi.org/10.1093/nar/gkw257.
58. Servant, N., Varoquaux, N., Lajoie, B.R., Viara, E., Chen, C.J., Vert, J.P., Heard, E., Dekker, J., and Barillot, E. (2015). HiC-Pro: an optimized and flexible pipeline for Hi-C data processing. Genome Biol. *16*, 259. https://doi.org/10.1186/s13059-015-0831-x.
59. Kruse, K., Hug, C.B., Hernández-Rodríguez, B., and Vaquerizas, J.M. (2016). TADtool: visual parameter identification for TAD-calling algorithms. Bioinformatics *32*, 3190–3192. https://doi.org/10.1093/bioinformatics/btw368.
60. Hao, Y., Hao, S., Andersen-Nissen, E., Mauck, W.M., 3rd, Zheng, S., Butler, A., Lee, M.J., Wilk, A.J., Darby, C., Zager, M., et al. (2021). Integrated analysis of multimodal single-cell data. Cell *184*, 3573–3587.e29. https://doi.org/10.1016/j.cell.2021.04.048.
61. Livak, K.J., and Schmittgen, T.D. (2001). Analysis of relative gene expression data using real-time quantitative PCR and the 2(-Delta Delta C(T) Method. Methods *25*, 402–408. https://doi.org/10.1006/meth.2001.1262.
62. Ahmad, K., and Henikoff, S. (2020). CUT&Tag with Drosophila tissues. Protocols.io. https://doi.org/10.17504/protocols.io.bnx5mfq6.
63. Ahmad, K., and Henikoff, S. (2021). The H3.3K27M oncohistone antagonizes reprogramming in Drosophila. PLoS Genet. *17*, e1009225. https://doi.org/10.1371/journal.pgen.1009225.
64. Matelot, M., and Noordermeer, D. (2016). Determination of high-resolution 3D chromatin organization using circular chromosome conformation capture (4C-seq). Methods Mol. Biol. *1480*, 223–241. https://doi.org/10.1007/978-1-4939-6380-5_20.
65. David, F.P.A., Delafontaine, J., Carat, S., Ross, F.J., Lefebvre, G., Jarosz, Y., Sinclair, L., Noordermeer, D., Rougemont, J., and Leleu, M. (2014). HTSstation: a web application and open-access libraries for high-throughput sequencing data analysis. PLoS One *9*, e85879. https://doi.org/10.1371/journal.pone.0085879.

STAR★METHODS

KEY RESOURCES TABLE

REAGENT or RESOURCE	SOURCE	IDENTIFIER
Antibodies		
H3K4me3	Merck-Millipore	07-473; RRID: AB_1977252
H3K27me3	Merck-Millipore	17-622; RRID: AB_916347
Critical commercial assays		
NEBNext Ultra II FS DNA library kit	New England Biolabs	E7805S
SuperScript IV First strand synthesis System	ThermoFisher Scientific	18091050
SsoAdvanced Universal SYBR Green mix	BioRad	1725270
Expand Long Template PCR system	Roche	11759060001
Chromium Next GEM Single Cell 3' kit v3.1	10X Genomics	PN-1000128
Chromium Next GEM Single Cell 5' Kit v2	10X Genomics	PN-1000265
Arima-HiC+ for HiC kit	Arima Genomics	N/A
Deposited data		
Hi-C - S2 cells	Szabo et al., 2018[44]	GEO: GSE99107
ChIP-seq dCTCF - S2 cells	Ong et al., 2013[38]	GEO: GSE41354
ChIP-seq CP190 - S2 cells	Ong et al., 2013[38]	GEO: GSE41354
ChIP-seq dCTCF - whole embryo	Kaushal et al., 2022[39]	GEO: GSE180376
ChIP-seq CP190 - whole embryo	Kaushal et al., 2022[39]	GEO: GSE180376
ChIP-seq dCTCF - larval central nervous system	Kaushal et al., 2021[40]	GEO: GSE146752
ChIP-seq CP190 - larval central nervous system	Kaushal et al., 2021[40]	GEO: GSE146752
ChIP-seq H3K4me3 - S2 cells	This study	ENA: PRJEB52393 Mendeley Data: https://doi.org/10.17632/rs4sns574p.1
ChIP-seq H3K27me3 - S2 cells	This study	ENA: PRJEB52393 Mendeley Data: https://doi.org/10.17632/rs4sns574p.1
ChIP-seq H3K4me3 - S3 cells	This study	ENA: PRJEB52393 Mendeley Data: https://doi.org/10.17632/rs4sns574p.1
ChIP-seq H3K27me3 - S3 cells	This study	ENA: PRJEB52393 Mendeley Data: https://doi.org/10.17632/rs4sns574p.1
ChIP-seq H3K4me3 - Sg4 cells	This study	ENA: PRJEB52393 Mendeley Data: https://doi.org/10.17632/rs4sns574p.1
ChIP-seq H3K27me3 - Sg4 cells	This study	ENA: PRJEB52393 Mendeley Data: https://doi.org/10.17632/rs4sns574p.1
ChIP-seq H3K4me3 - genital discs w1118	This study	ENA: PRJEB52393 Mendeley Data: https://doi.org/10.17632/rs4sns574p.1
ChIP-seq H3K4me3 - genital discs Fab-7[1]	This study	ENA: PRJEB52393 Mendeley Data: https://doi.org/10.17632/rs4sns574p.1
4C-seq for different viewpoints - S2, S3, Sg4 and Kc167 cells, and genital and wing discs	This study	ENA: PRJEB52393
Hi-C - Sg4 cells	This study	ENA: PRJEB52393 Mendeley Data: https://doi.org/10.17632/rs4sns574p.1
Single cell RNA-seq data - imaginal discs	This study	ENA: PRJEB52393 Mendeley Data: https://doi.org/10.17632/rs4sns574p.1

(*Continued on next page*)

Continued

REAGENT or RESOURCE	SOURCE	IDENTIFIER
Experimental models: Cell lines		
Kc167 cells	Gift from Matthieu Sanial, Institut Jacques Monod (France)	FlyBase: FBtc0000001
S3 cells	Drosophila Genomics Resource Center (DGRC, USA)	FlyBase: FBtc0000005
S2 cells	Drosophila Genomics Resource Center (DGRC, USA)	FlyBase: FBtc0000006
Sg4 cells	Drosophila Genomics Resource Center (DGRC, USA)	FlyBase: FBtc0000179
Experimental models: Organisms/strains		
Dmel\Fab7[1]	Gift from François Karch, University of Geneva (Switzerland)	FlyBase: FBal0028656
Dmel\w[1118]	Gift from Jacques Montagne, Institute for Integrative Biology of the Cell (France)	FlyBase: FBal0018186
Oligonucleotides		
Listed in Table S2	This study	N/A
Software and algorithms		
C4CTUS	Miranda et al., 2022[54]	https://github.com/NoordermeerLab/c4ctus
bowtie2	Langmead et al., 2012[55]	http://bowtie-bio.sourceforge.net/bowtie2/index.shtml
SAMtools	Danecek et al., 2021[56]	http://www.htslib.org/
BAMCoverage	Ramírez et al., 2016[57]	https://deeptools.readthedocs.io/en/develop/content/tools/bamCoverage.html
HiC-Pro	Servant et al., 2015[58]	https://github.com/nservant/HiC-Pro
TADtool	Kruse et al., 2016[59]	https://github.com/vaquerizaslab/tadtool
Cell Ranger software	10X Genomics	https://support.10xgenomics.com/single-cell-gene-expression/software/pipelines/latest/what-is-cell-ranger
Loupe browser	10X Genomics	https://support.10xgenomics.com/single-cell-vdj/software/visualization/latest/what-is-loupe-browser
Seurat tool	Hao et al., 2021[60]	https://satijalab.org/seurat/
Excel Spreadsheet software	Microsoft Corporation	https://www.microsoft.com/en-us/microsoft-365/excel
G-test of independence Excel spreadsheet	Handbook of Biological Statistics	http://www.biostathandbook.com/gtestind.html

RESOURCE AVAILABILITY

Lead contact

Further information and requests for resources and reagents should be directed to and will be fulfilled by the lead contact Daan Noordermeer (daan.noordermeer@i2bc.paris-saclay.fr).

Materials availability

This study did not generate new unique reagents.

Data and code availability

- All unprocessed Illumina sequencing data generated in this study (Hi-C, ChIP-seq, 4C-seq and single-cell RNA-seq) have been deposited in the European Nucleotide Archive (EMBL-EBI ENA): PRJEB52393. Processed Hi-C, ChIP-seq and single-cell RNA-seq data are available from Mendeley Data: https://doi.org/10.17632/rs4sns574p.1. Processed 4C-seq data is available from the lead contact upon request.
- This paper does not report original code.
- Any additional information required to reanalyze the data reported in this paper is available from the lead contact upon request.

EXPERIMENTAL MODEL AND SUBJECT DETAILS

Fly strains

WT flies (w^{1118} background) were a gift from Jacques Montagne (I2BC, France). $Fab7^{1}$ deletion flies were a gift from François Karch (University of Geneva, Switzerland). In $Fab7^{1}$ flies, a 4.3 kb region between *Abd-B* and *abd-A* that contains the Fab-7 element is absent.[27] Fly stocks were maintained and cultured using standard cornmeal yeast extract medium at 25°C.

Cell lines

The S2, Sg4 and S3 cell lines were ordered from Drosophila Genomics Resource Center (Indiana University, USA). The Kc167 cell line was a gift from Matthieu Sanial (IJM, France). S2 cells were grown in Schneider medium (ThermoFisher Scientific). Sg4, S3 and Kc167 cells were grown in M3+BPYE medium (Sigma-Aldrich). Culture mediums were supplemented with 1% penicillin/streptomycin (ThermoFisher Scientific) and different amounts of Fetal Bovine Serum (FBS): 10% for S2 cells; 12.5% for the Sg4, S3 and Kc167 cells). Conventional Gibco FBS was used (ThermoFisher Scientific) for S2 and S3 cells, whereas Gibco Performance FBS was used for Sg4 and Kc167 cells. Cells were inoculated at 1 - 3 million cells/ ml, grown at 25°C and split every 2-4 days.

METHODS DETAILS

RT-qPCR

3 - 5 million cells were lysed in 1 ml Trizol (ThermoFisher Scientific) and total RNA was purified using the NucleoSpin RNA kit (Macherey-Nagel). Reverse-transcription (RT) was performed using SuperScript IV and Random hexamers following the manufacturer's instructions (ThermoFisher Scientific). A similar protocol was followed for whole larvae (20 L3 larvae) and larval imaginal discs (50 wing discs or 150 genital discs). For whole embryos, flies were allowed to lay embryos for 2 hours on yeasted grape juice plates at 25°C, after 2 hours of pre-collection. Plates were incubated at 25°C for 16 hours. The resulting embryos were dechorionated for 1.5. minutes using bleach, followed by several rinses with 1X PBS and transfer to 1 mL Trizol (ThermoFisher Scientific). Embryos were dissociated using a pestle, followed by RNA isolation and RT as described above. Between 88 ng and 1 μg total RNA was used for the all the RT reactions.

cDNA was amplified using SsoAdvanced Universal SYBRGreen Supermix (BioRad) and 0.5 μM of corresponding primers. With the exception of the *Abd-B* C promoter, primers were designed over intron boundaries to prevent amplification from genomic DNA using the online version of Primer3 software (https://primer3.ut.ee/). Primers were annealed at 55°C or 60°C and Real-time PCR was performed using a LightCycler 480 instrument (Roche). mRNA abundance was normalized to the *Gapdh2* and *Act42A* housekeeping genes using the ΔΔCt method.[61] Primer sequences for RT-qPCR amplification are listed in Table S2.

Calibrated RT-qPCR for absolute quantification of Abd-B isoforms

To determine absolute mRNA abundance of *Abd-B* isoforms, external calibration was performed using a plasmid containing all *Abd-B* isoform-specific RT-qPCR amplicons. The plasmid was assembled using the NEBuilder HiFi DNA Assembly kit (NEB) into a linearized pBlueScript backbone using larval cDNA as a template. Primer sequences for Gibson assembly are listed in Table S2. Primers were annealed at 55°C or 60°C and qPCR was performed using the SsoAdvanced Universal SYBR Green Supermix (BioRad) on a LightCycler 480 instrument (Roche). mRNA abundance for the different isoforms was normalized over the reference plasmid and a primer set to the common exon of all isoforms. Experiments were performed on biological duplicates (n=2). Primer sequences for RT-qPCR amplification are listed in Table S2.

ChIP-seq and ChIP-qPCR

50 million S2, Sg4 or S3 cells were cross-linked in 1% formaldehyde for 10 min at room temperature. After quenching the cross-link reaction by adding 125 mM glycine, cells were lysed sequentially in buffers containing 10% Glycerol, 50 mM Tris-HCl pH 8.0, 140 mM NaCl, 1 mM EDTA, 0.5 % NP-40, 0.25 % Triton X-100 and 0.33X Complete Protease Inhibitors (Roche), followed by a buffer containing 10 mM Tris-HCl pH 7.5, 200 mM NaCl, 1 mM EDTA and 0.33X Complete Protease Inhibitors and a buffer containing 10 mM Tris-HCl pH 7.5, 100 mM NaCl, 1 mM EDTA, 0.25% SDS, 0.1% NaDeoxycholate and 1X Complete Protease Inhibitors. Chromatin was sheared using a Covaris S220 device with the following parameters: Peak Power: 110W, Duty Factor: 15%, Cycles/burst: 200, Duration: 1200 sec. After clarification by centrifugation, aliquots of sheared chromatin were kept at -80°C.

For ChIP experiments, 3 μg of sonicated chromatin was diluted in a buffer containing 16 mM Tris-HCl pH 8.0, 167 mM NaCl, 1.2 mM EDTA, 0.01% SDS, 1.1% Triton X-100 and 1x Complete Protease Inhibitors (Roche) and precleared with Salmon Sperm DNA/Protein A Agarose beads (Merck-Millipore) for 30 min at 4°C. 10% of the sample was taken as input sample and the remainder was incubated with the specific antibody overnight at 4°C. The following antibodies were used: 2 μL H3K4me3 (07-473, Merck-Millipore) or 5 μg H3K27me3 (17-622, Merck-Millipore). Antibody-bound chromatin was isolated using Salmon Sperm DNA/Protein A Agarose beads, followed by sequential washing with Low Salt Immune Complex Wash Buffer (20 mM Tris-HCl pH 8.0, 150 mM NaCl, 2 mM EDTA, 0.1 % SDS and 1 % Triton X-100), High Salt Immune Complex Wash Buffer (20 mM Tris-HCl pH 7.5, 500 mM NaCl, 2mM EDTA, 0.1 % SDS, 1 % Triton X-100), LiCl Immune Complex Wash Buffer (10 mM Tris-HCl pH 7.5, 1 mM EDTA, 0.26 M LiCl, 2% NP-40 and Na Deoxycholate) and twice in 10mM Tris-HCl, 1mM EDTA. Chromatin was eluted using a 1% SDS, 0.1 mM $NaHCO_3$ solution, followed by decrosslinking.

For ChIP-qPCR, experiments were performed using the SsoAdvanced Universal SYBR Green Supermix (BioRad) on a LightCycler 480 instrument (Roche). Enrichment was determined relative to Input using the ΔCt method. Primer sequences for ChIP-qPCR amplification are listed in Table S2.

For ChIP-seq, Illumina sequencing libraries were prepared using the NEBNext Ultra II FS DNA library kit (NEB) and sequenced on the Illumina NextSeq 500 or 550 system (75 bp single end reads). ChIP-seq sequencing reads were filtered using FastQC filtering (https://www.bioinformatics.babraham.ac.uk/projects/fastqc/), followed by mapping onto the *Drosophila* genome (dm6) using bowtie2 (version 2.3.0) with filtering for multiple alignments.[55] Low quality reads (<30) and PCR duplicates were removed using SAMtools.[56] Bedgraphs were generated using BAMCoverage.[57] Published CP190 and dCTCF ChIP-seq data in S2 cells,[38] whole embryo[39] and larval central nervous system[40] were analyzed using the same strategy.

CUT&Tag

CUT&Tag for H3K4me3 and H3K27me3 on WT and Fab-7 mutant genital discs was performed as described,[62,63] with the following modifications. Larvae were harvested and washed in 1X PBS and then transferred to a buffer containing 20 mM HEPES pH 7.5, 150 mM NaCl, 0.5 mM Spermidine and 1X Complete Protease Inhibitors (Roche). 80 genital discs per genotype were dissected and collected in 200 μL of the same buffer, followed by addition of 10 μL Concanavalin A-coated beads suspension. After a 10 min incubation, the solution was removed and discs were incubated O/N at 4°C in 50 μL of 1% diluted H3K4me3 (07-473, Merck-Millipore) or H3K27me3 (17-622, Merck-Millipore) antibody. After removal of the diluted antibody solution, discs were incubated for 40 minutes in 50 μL of 1% secondary antibody solution. For the CUT&Tag reaction, the discs were first incubated for 1 hour in 50 μL of home-made pAG-Tn5 (IJM, France). Discs were then washed with 50 μL of a buffer containing 20 mM HEPES pH 7.5, 300 mM NaCl, 0.5 mM Spermidine and 1X Complete Protease Inhibitors followed by tagmentation for 1 hour at 37°C in 50 μL of a buffer containing 10mM $MgCl_2$, 20 mM HEPES pH 7.5, 300 mM NaCl, 0.5 mM Spermidine and 1X Complete Protease Inhibitors. The reaction was stopped by adding 50 μL of a buffer containing 0.17% SDS, 0.3 mg Proteinase K, 20 mM HEPES pH 7.5, 300 mM NaCl, 0.5 mM Spermidine and 1X Complete Protease Inhibitors and incubation for 1 hour at 58°C. DNA was purified using phenol-chloroform-isoamyl alcohol extraction and ethanol precipitation. Libraries were amplified using the NEBNext High-Fidelity 2X PCR Master Mix (NEB). CUT&Tag libraries were sequenced on the Illumina Nextseq 550 system (75 bp paired end reads) and analyzed as described for the ChIP-seq data.

4C-seq

Suitable 4C viewpoints were selected within or near the promoter of selected genes based on previously published criteria and genomic sequences obtained from the *Drosophila* dm6 release.[64] PAGE-purified sequencing primers containing Illumina Tru-seq adapters and indexes (Eurogentec) are listed in Table S2.

4C-seq in cell lines was performed as published[64] with modifications: 50 million cells were cross-linked in 2% formaldehyde for 10 min at room temperature and lysed in a buffer containing 50 mM Tris-HCl pH 7.5, 150 mM NaCl, 5 mM EDTA, 0.5% NP-40, 1% Triton and 1X Complete Protease Inhibitors (Roche). After lysis, cell aliquots were stored at - 80°C. 4C-seq libraries were generated using DpnII (NEB) as first restriction enzyme and NlaIII (NEB) as the second restriction enzyme. Ligation reactions were performed using high concentration T4 DNA Ligase (Promega). For each viewpoint, 12 PCR reactions each containing 12 ng were performed using the Expand Long Template PCR System (Roche) with 30 cycles of amplification on a Thermocycler (Bio-Rad C1000). PCR reactions were pooled and purified using a PCR Clean up kit (Qiagen). Up to 23 viewpoints were mixed in equimolar ratio and sequenced on the Illumina NextSeq500 or 550 system (75 bp single end reads).

For 4C-seq in larval imaginal discs, a minimum of 1600 genital discs or 400 wing discs were dissected in cold 1X PBS over multiple sessions that lasted a maximum of 1 hour. Chromatin crosslinking and cell lysis were performed as for cell lines after dissection, with the addition of a second cell lysis step using a glass douncer with pestle. After lysis, cell aliquots were stored at - 80°C. After pooling of imaginal discs, the experimental procedure as outlined for cell lines was followed.

4C-seq sequencing reads were sorted, aligned, and translated to restriction fragments using the C4CTUS tool, which is a standalone version of the 4C-seq module within the former HTSstation online data analysis service.[54,65] Reads from different biological samples were demultiplexed using their Illumina Index and reads from different viewpoints were demultiplexed using the first 18 bases sequenced (viewpoint-specific primer). After removing the sequence of the viewpoint-specific primer, the remainder of the reads were mapped onto the *Drosophila* genome (dm6). Reads mapping to the viewpoint, the directly neighboring "undigested" fragment

and fragments 2 kb up- and downstream were excluded during the procedure. Fragment counts were normalized per one million reads in a region within chr3R:4,661,427-8,999,228 (for viewpoints in the ANT-C) or chr3R:14,656,623-18,972,236 (for viewpoints in the BX-C). For visualizations, all tracks were smoothed using a running mean transformation over 11 consecutive valid restriction fragments.

Hi-C

For Sg4 cells, Hi-C was performed on 15 million cells using the Arima Hi-C kit (Arima Genomics), following the manufacturer's instructions. Hi-C material was sequenced on the Illumina NovaSeq 6000 system (150 bp paired end reads). Hi-C data from S2 R+ cells were obtained from the GEO repository GSE99107.[44]

Hi-C reads were mapped to the *Drosophila* genome (dm6) using HiC-Pro (version 2.11.1) and bowtie2 (version 1.1.2).[55,58] Default settings were used to remove duplicates, assign reads to their restriction fragments and filter for valid interactions. Hi-C matrices at 5kb resolution were generated from the valid interactions and normalized with the Iterative Correction and Eigenvector decomposition method (ICE) in the HiC-Pro tool. TADtool was used to call TAD boundaries with a window size of 51kb and a cutoff of 47 (S2 cells) or 75 (Sg4 cells).[59]

Single-cell RNA-seq

For single-cell RNA-seq experiments on cell lines, one million S2 and Sg4 cells were diluted in PBS (without $MgCl_2$) and 0.04% BSA to a concentration of 1000 cells / µl. Reverse transcription and sequencing library preparation were done using the Chromium Next GEM Single Cell 3' kit (10X Genomics), according to the manufacturer's instructions. 3'- single-cell RNA-seq libraries were sequenced on the Illumina NextSeq 550 system (75 bp paired end reads).

For single-cell RNA-seq experiments on WT and Fab-7^1 larval imaginal discs, pools of discs were dissected within 20 min in PBS (without $MgCl_2$) with 0.04% BSA. To obtain roughly equivalent numbers of cells for each type of imaginal disc, the following pools of discs were combined: 4 eye/antenna discs, 8 leg-1 discs, 4 leg-2 discs, 4 leg-3 discs, 8 halter discs, 2 wing discs and 16 genital discs. Pools of discs were dissociated in 0.05% Trypsin EDTA (Thermofisher Scientific) for 8 minutes at 37°C and resuspended in PBS (without $MgCl_2$) with 0.04% BSA to a concentration of approximately 1000 cells / µl. Reverse transcription and sequencing library preparation were done using the Chromium Next GEM Single Cell 5' kit (10X Genomics), according to the manufacturer's instructions. 5'- single-cell RNA-seq libraries were sequenced on the Illumina NextSeq 550 system (75 bp paired end reads).

FastQ files were analyzed using the Cell Ranger software (10X Genomics, version 3.1.0), including alignment, filtering and quantitation of reads on the *Drosophila* genome (dm6) and generation of feature-barcode matrices. For the Sg4 and S2 cell lines, the clusters were obtained using k-means clustering (k = 3) using the Cell Ranger software. Further visualizations were generated using the Loupe browser (10X Genomics, version 4.2.0). For the imaginal discs, all downstream analyses were performed using the Seurat tool (version 4.0.1).[60] Cells with UMI count lower than 350 and mitochondrial genes above 5.5% were excluded from the analysis. After log-normalization, the vst method was used to select the top 2,000 variable features. WT and Fab-7^1 imaginal disc cell data were then integrated using the dataset with the highest number of cells and the first 10 dimensions as a reference. Clustering was performed with the functions FindNeighbors and FindClusters, using the first 10 dimensions from PCA, resulting in the identification of 14 clusters. Identification of the clusters was done using the FindConservedmarkers function in Seurat. Cluster identities were assigned based on *Hox* gene expression for imaginal discs whereas for neurons, muscle and dead cells, the identities were assigned using the Flybase database. Muscle cells and genital discs were initially assigned to two clusters each, which we merged for further analysis. All visualizations were performed using Seurat as well.

QUANTIFICATION AND STATISTICAL ANALYSIS

Details of statistical analyses performed in this paper including analyses packages can be found in the figure legends and STAR Methods. Standard deviations for RT-qPCR and calibrated RT-qPCR experiments were calculated on combined measurements from biological and technical replicates using Microsoft Excel. For all experiments, at least two measurements (independent qPCR experiments) were performed on each of the biological replicates (RNA isolates from independent groups of embryos and larvae or independent cell culture experiments). Significance of difference between samples was determined using the t test function in Microsoft Excel. The number of biological replicates is indicated in the figure legends.

To determine the significance of difference between the bins with increased signal in CUT&Tag experiments (Figure 4B), we compared the number of bins with increases and decreased signal between cell types using a G test of independence (see key resources table). To determine the significance of difference between the number of cells where *Abd-B* isoforms were detected in the single-cell RNA-seq analysis (Figure 5B), we compared the number of cells with and without detected isoforms between cell types using a G test of independence (see key resources table).

Cell Reports, Volume *42*

Supplemental information

The *Drosophila* Fab-7 boundary modulates *Abd-B* gene activity by guiding an inversion of collinear chromatin organization and alternate promoter use

Laura Moniot-Perron, Benoit Moindrot, Line Manceau, Joanne Edouard, Yan Jaszczyszyn, Pascale Gilardi-Hebenstreit, Céline Hernandez, Sébastien Bloyer, and Daan Noordermeer

Figure S1: Histone modification landscape of the ANT-C and BX-C. Related to Figure 1.

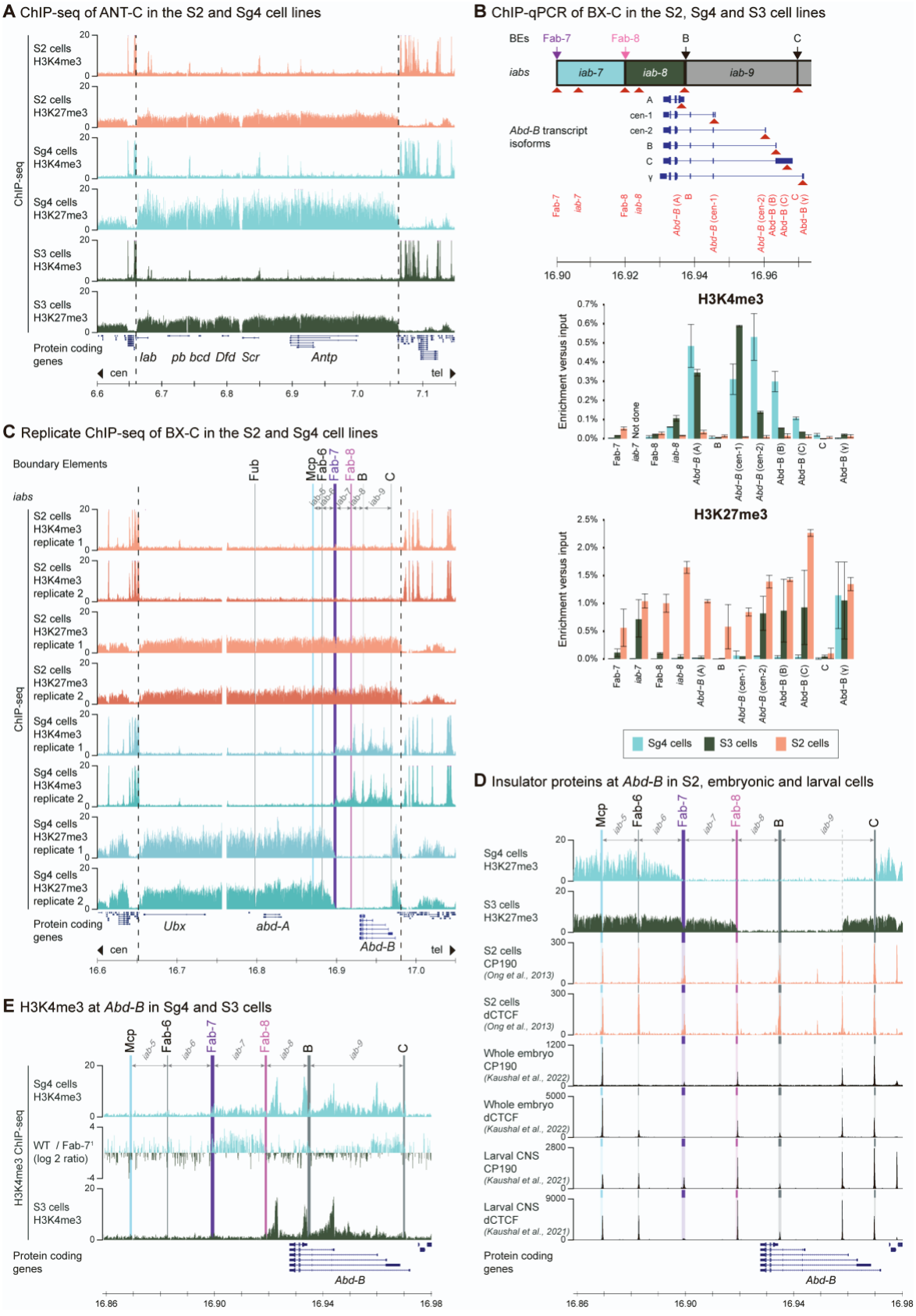

Figure S1: Histone modification landscape of the ANT-C and BX-C. Related to Figure 1.

A. ChIP-seq data for the H3K4me3 and H3K27me3 histone marks in the S2, Sg4 and S3 cell lines at the ANT-C. The ANT-C is demarcated by dashed lines. Location of protein coding transcripts is indicated below.

B. ChIP-qPCR for the H3K27me and H3K4me3 histone marks in the Sg4, S3 and S2 cell lines. Data are normalized over input. The position of analyzed regions within the *Abd-B cis*-regulatory domain is indicated above (red arrow heads). Data based on biological replicates (n = 2). Error bars indicate Standard Deviation.

C. ChIP-seq data for the H3K4me3 and H3K27me3 histone marks at the BX-C in biological replicates for the S2 and Sg4 cell lines.

D. Zoom-in of reanalyzed ChIP-seq data for the CP190 and dCTCF insulator proteins in the S2 cell line, whole embryo and in the Central Nervous System of larvae over the *Abd-B cis*-regulatory domain. ChIP-seq data for H3K27me3 in the Sg4 and S3 cell lines is indicated above. BEs and *iabs* relevant for *Abd-B* regulation are indicated on top. Location of protein coding transcripts is indicated below.

E. Zoom-in of H3K4me3 ChIP-seq data in the Sg4 and S3 cell lines over the *Abd-B cis*-regulatory domain. The log2 ratio of ChIP-seq signal (50 bp bins) is indicated in-between the tracks. BEs and *iabs* relevant for *Abd-B* regulation are indicated on top. Location of protein coding transcripts is indicated below.

Figure S2: 3D chromatin organization of the ANT-C and BX-C in repressed cell types. Related to Figure 2.

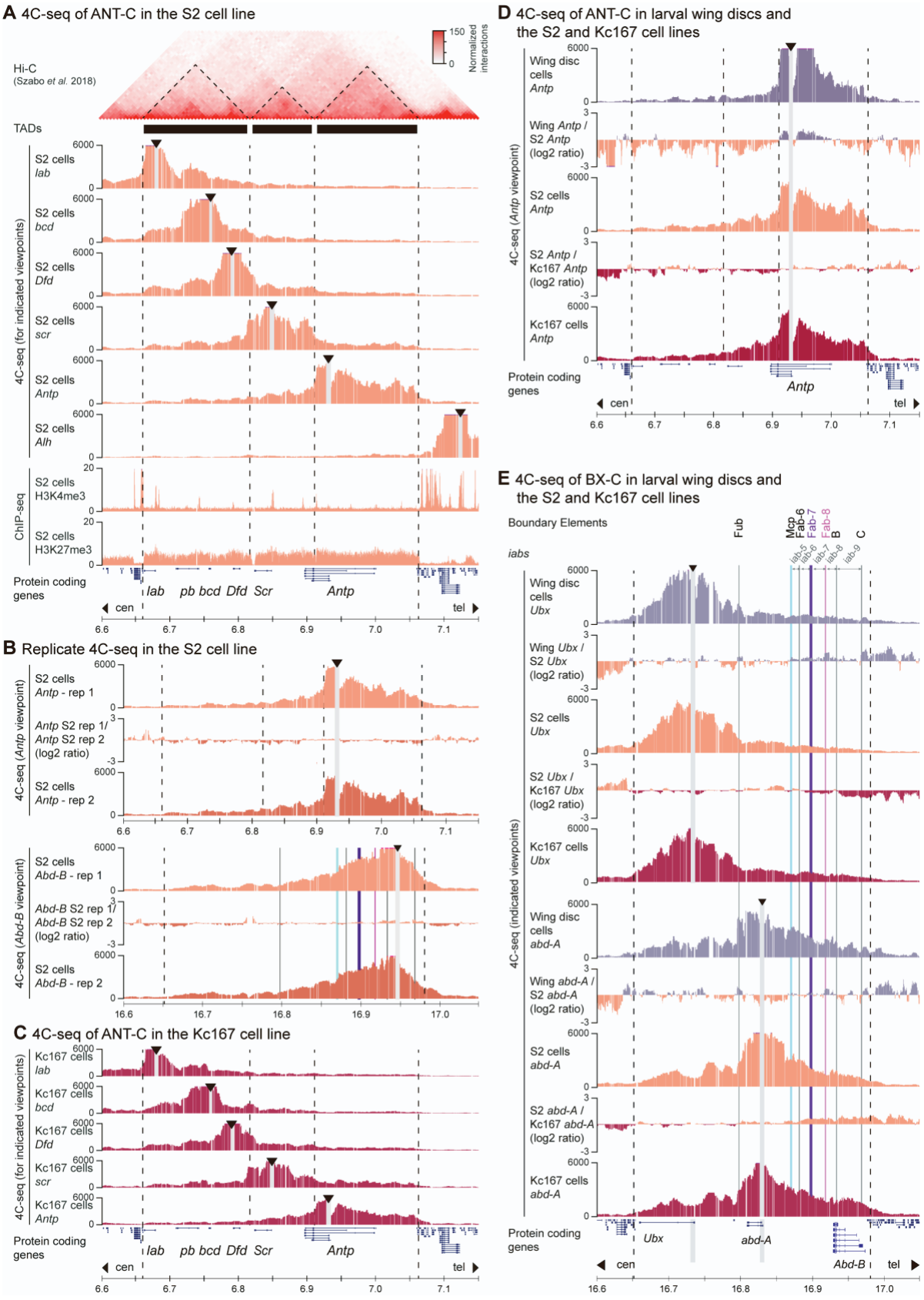

Figure S2: 3D chromatin organization of the ANT-C and BX-C in repressed cell types. Related to Figure 2.

A. Hi-C (top), 4C-seq (middle) and ChIP-seq (bottom) data for the ANT-C in the S2 cell line. Hi-C data was reanalyzed from [S1], with identified sub-domains indicated as black bars. 4C-seq data for viewpoints in the promoters of the *Lab, bcd, Dfd, Scr, Antp* and *Alh* genes is indicated in-between. H3K4me3 and H3K27me3 ChIP-seq data is indicated below. The ANT-C is demarcated by dashed lines. Location of protein coding transcripts is indicated below. Arrowheads indicate the positions of viewpoints.

B. 4C-seq data in biological replicates for the S2 cell line for the indicated viewpoints. In-between, the log2 ratio of interactions is shown.

C. 4C-seq data for the ANT-C in the Kc167 cell line for the indicated viewpoints. Location of protein coding transcripts is indicated below.

D. 4C-seq data in wing disc cells and the S2 and Kc167 cell lines for the *Antp* viewpoint. In-between, the log2 ratio of interactions is shown. Location of protein coding transcripts is indicated below.

E. 4C-seq data in wing disc cells and the S2 and Kc167 cell lines for the *Ubx* and *abd-A* viewpoints. In-between, the log2 ratio of interactions is shown. The BX-C is demarcated by dashed lines, with known BEs highlighted by vertical bars. BEs and *iabs* relevant for *Abd-B* regulation are indicated on top. Location of protein coding transcripts is indicated below.

Figure S3: 3D chromatin organization of the ANT-C and BX-C in cell types where *Abd-B* is active. Related to Figure 3.

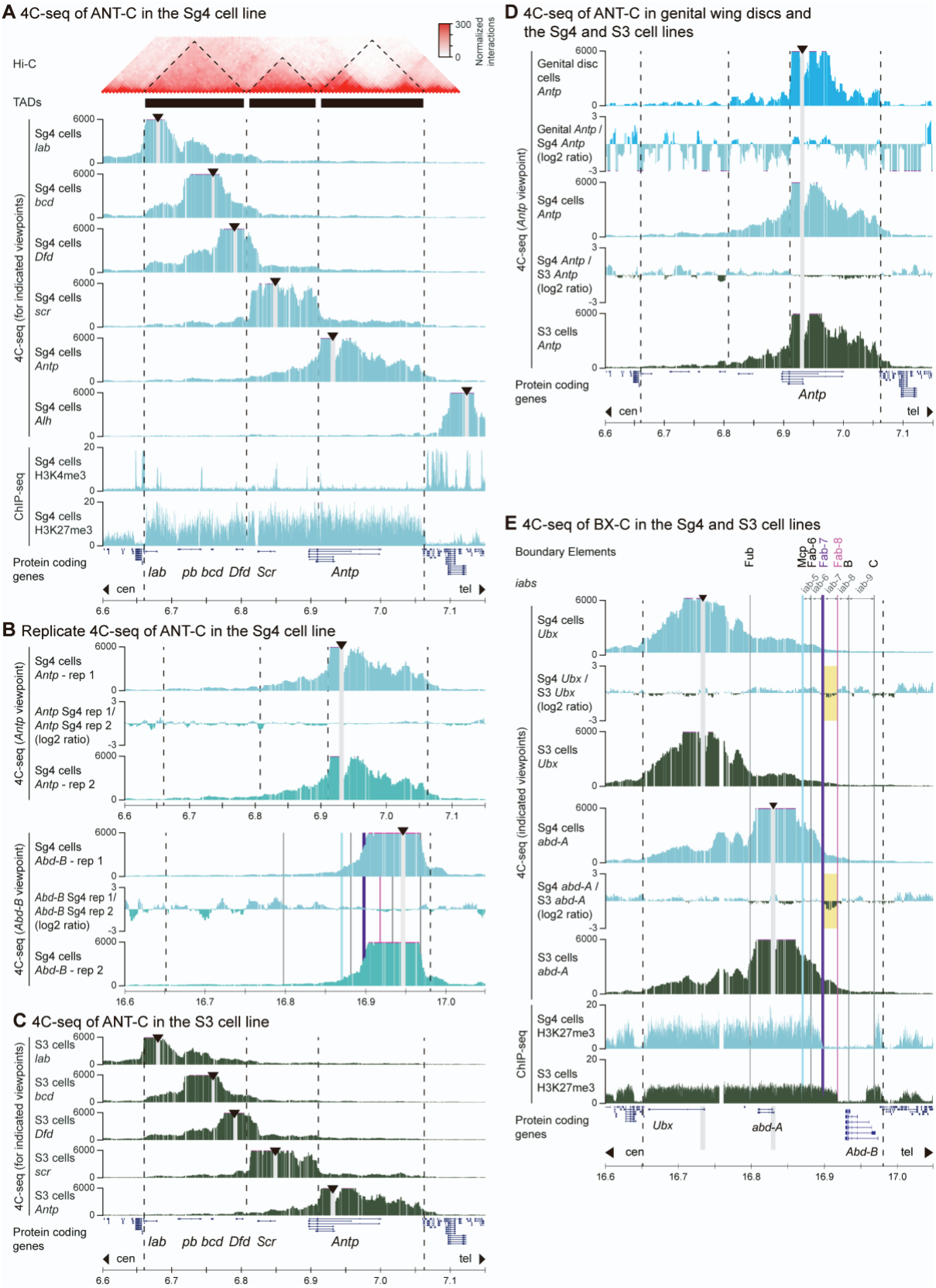

Figure S3: 3D chromatin organization of the ANT-C and BX-C in cell types where *Abd-B* is active. Related to Figure 3.

A. Hi-C (top), 4C-seq (middle) and ChIP-seq (bottom) data for the ANT-C in the Sg4 cell line. Sub-domains as identified by Hi-C are indicated as black bars. 4C-seq data for viewpoints in the promoters of the *Lab, bcd, Dfd, Scr, Antp* and *Alh* genes is indicated in-between. H3K4me3 and H3K27me3 ChIP-seq data is indicated below. The ANT-C is demarcated by dashed lines. Location of protein coding transcripts is indicated below. Arrowheads indicate the positions of viewpoints.

B. 4C-seq data in biological replicates for the Sg4 cell line for the indicated viewpoints. In-between, the log2 ratio of interactions is shown.

C. 4C-seq data for the ANT-C in the S3 cell line for the indicated viewpoints. Location of protein coding transcripts is indicated below.

D. 4C-seq data in genital disc cells and the Sg4 and S3 cell lines for the *Antp* viewpoint. In-between, the log2 ratio of interactions is shown. Location of protein coding transcripts is indicated below.

E. 4C-seq data in the Sg4 and S3 cell lines for the *Ubx* and *abd-A* viewpoints. In-between, the log2 ratio of interactions is shown. Yellow rectangles highlight the domain of reduced interactions in Sg4 cells that overlaps the *iab-7*. The BX-C is demarcated by dashed lines, with known BEs highlighted by vertical bars. BEs and *iabs* relevant for *Abd-B* regulation are indicated on top. Location of protein coding transcripts is indicated below.

Figure S4: 3D chromatin organization of the repressed BX-C in WT and Fab-7[1] deletion wing disc cells. Related to Figure 4.

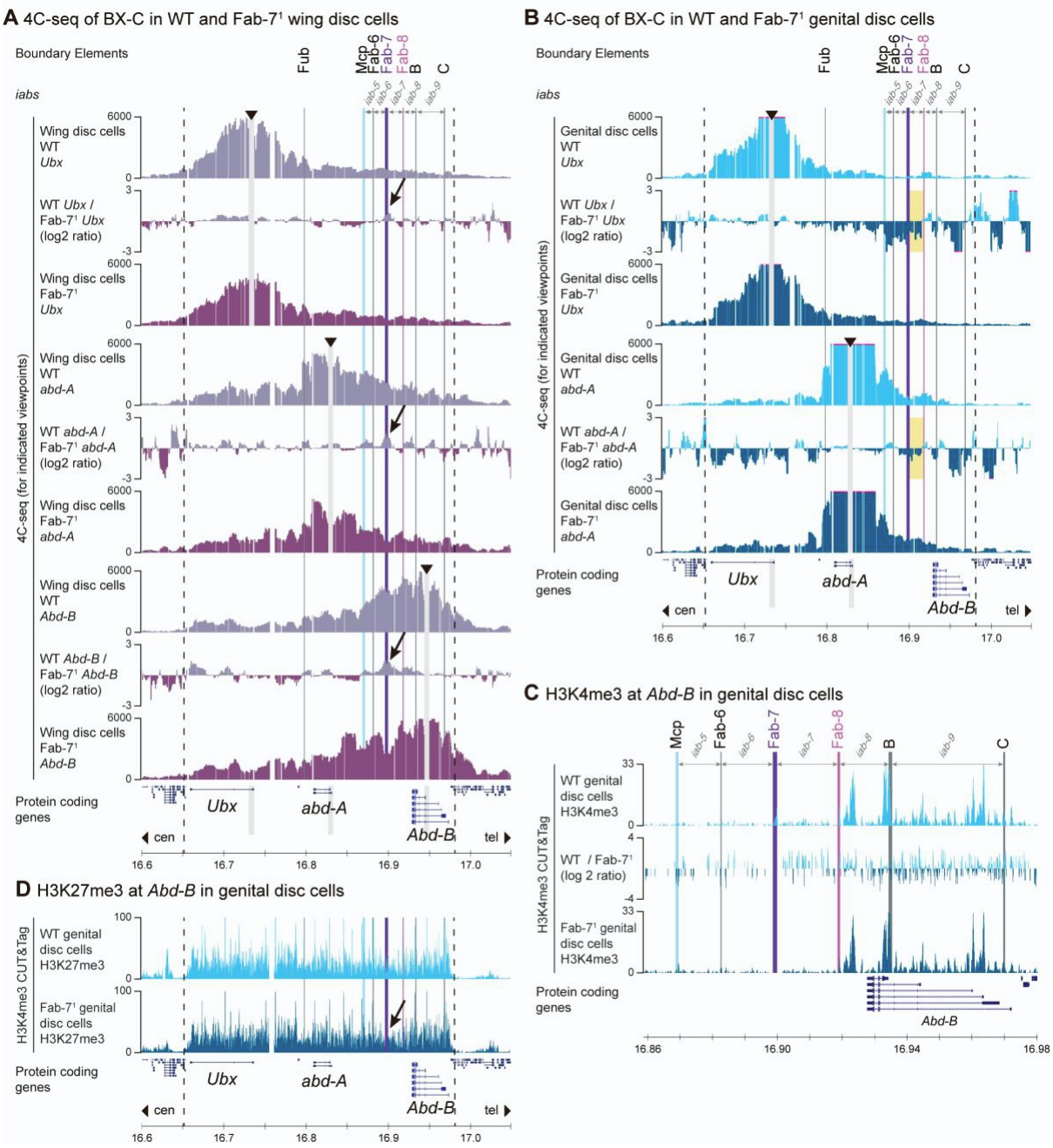

Figure S4: 3D chromatin organization of the repressed BX-C in WT and Fab-7^{1} deletion wing disc cells. Related to Figure 4.

A. 4C-seq data in WT and Fab-7^{1} deletion wing disc cells for the *Ubx, abd-A* and *Abd-B* viewpoints. In-between, the log2 ratio of interactions is shown. Black arrows indicate the gain of signal in the WT cells where the Fab-7 element is present. The BX-C is demarcated by dashed lines, with known BEs highlighted by vertical bars. BEs and *iabs* relevant for *Abd-B* regulation are indicated on top. Location of protein coding transcripts is indicated below. Arrowheads indicate the positions of viewpoints.

B. 4C-seq data in WT and Fab-7^{1} deletion genital disc cells for the *Ubx* and *abd-A* viewpoints. In-between, the log(2) ratio of interactions is shown. Yellow rectangles highlight the domain of reduced interactions in WT cells that overlaps the *iab-7*. The BX-C is demarcated by dashed lines, with known BEs highlighted by vertical bars. BEs and *iabs* relevant for *Abd-B* regulation are indicated on top. Location of protein coding transcripts is indicated below.

C. Zoom-in of H3K4me3 CUT&Tag data in WT and Fab-7^{1} deletion genital disc cells over the *Abd-B cis*-regulatory domain. The log2 ratio of CUT&Tag signal (50 bp bins) is indicated in-between the tracks. BEs and *iabs* relevant for *Abd-B* regulation are indicated on top. Location of protein coding transcripts is indicated below.

D. H3K27me3 CUT&Tag data in WT and Fab-7^{1} deletion genital disc cells. Black arrows indicate the loss of signal in the Fab-7^{1} deletion cells where the Fab-7 element is absent. The BX-C is demarcated by dashed lines, with known BEs highlighted by vertical bars. Location of protein coding transcripts is indicated below.

Figure S5: BX-C gene and promoter activity in individual cells. Related to Figure 5.

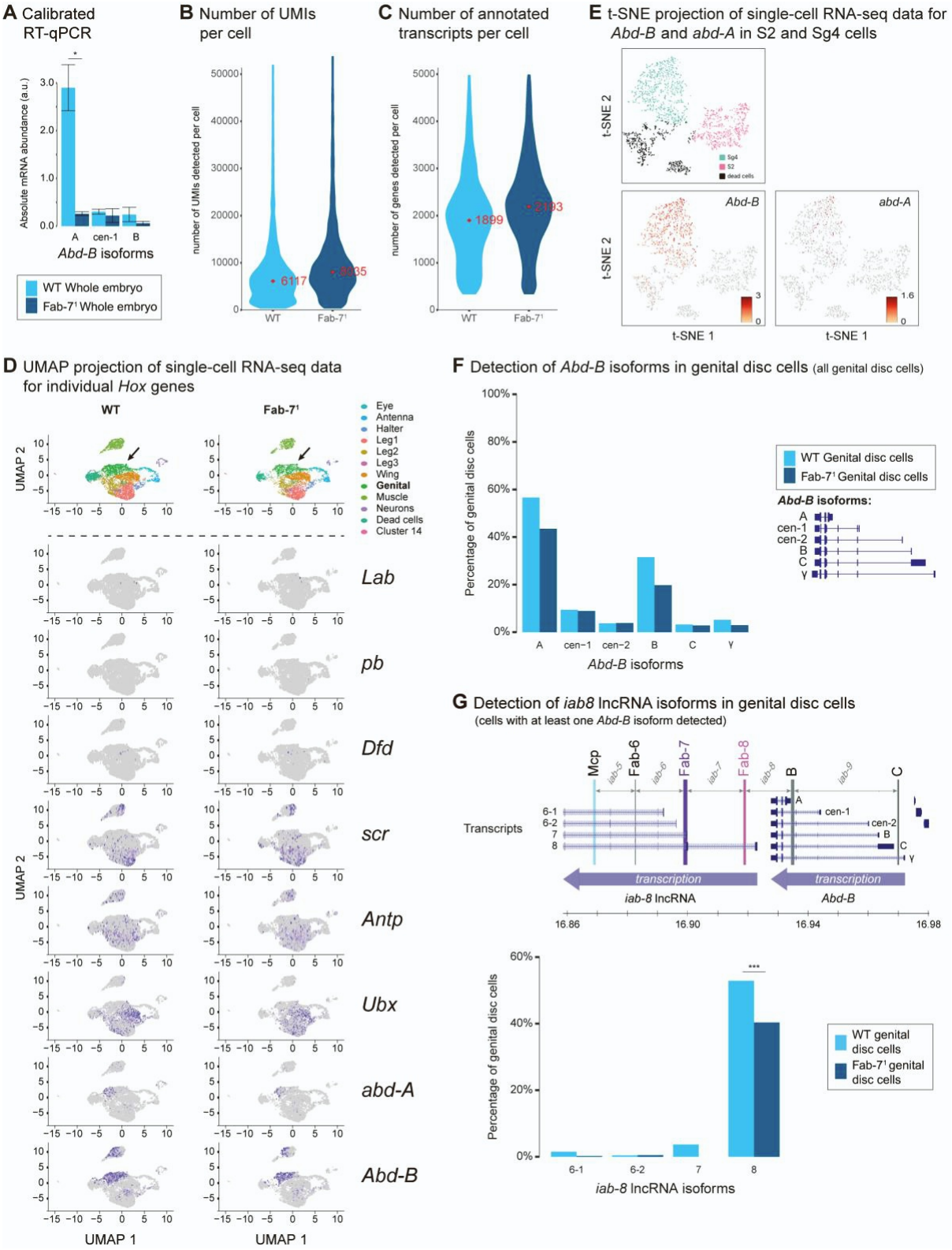

Figure S5: BX-C gene and promoter activity in individual cells. Related to Figure 5.

A. Calibrated RT-qPCR to quantify the activity of selected *Abd-B* promoters in WT and Fab-7 deletion whole embryos. Data are calibrated relative to a shared exon between all isoforms and to an external plasmid containing the isoform specific amplificons. Data based on biological replicates (n = 2). Error bars indicate Standard Deviation.

B. Violin plots showing the number of detected Unique Molecular Identifiers (UMIs) per cell in single-cell RNA-seq data from pools of WT and Fab-7^{1} deletion imaginal disc cells. Red diamonds and numbers indicate the median.

C. Violin plots showing the number of detected genes per cell in single-cell RNA-seq data from pools of WT and Fab-7^{1} deletion imaginal disc cells. Red diamonds and numbers indicate the median.

D. UMAP projections of single-cell RNA-seq data from pools of WT and Fab-7^{1} deletion imaginal disc cells. On the top, the identified clusters are indicated. On the bottom, the presence of mRNA from individual *Hox* genes (purple) within the pool of discs is indicated.

E. t-SNE projections of 3'- single-cell RNA-seq data from the combined S2 and Sg4 cell lines. On the top, the identified clusters are indicated. On the bottom, the detection of *Abd-B* or *abd-A* mRNA is indicated.

F. Histogram showing the percentage of cells where mRNA for each *Abd-B* isoform is detected in genital disc cells (percentages within the entire population of genital disc cells, including those where no *Abd-B* mRNA is detected).

G. Single-cell RNA-seq analysis of the *iab-8* lncRNA in WT and Fab-7 deletion genital disc cells. On top, the positions of the alternative promoters for the *iab-8* lncRNA and *Abd-B* gene within the *Abd-B cis*-regulatory domain are indicated. BEs and *iabs* relevant for *Abd-B* regulation are indicated as well. Below, a histogram showing the percentage of cells where mRNA from the indicated *iab-8* lncRNA promoters is detected (percentages in the population of genital disc cells where at least one isoform of *Abd-B* is detected). G-test: *** $p < 0.001$.

Table S1: single-cell RNA-seq results. Related to Figure 5.

Genital disc cells:

		WT								
		lab	***pb***	***Dfd***	***scr***	***Antp***	***Ubx***	***abd-A***	***Abd-B***	
		1.2%	0.0%	0.6%	0.0%	0.0%	0.00%	0.0%	0.2%	***lab***
			0.4%	0.1%	0.0%	0.0%	0.1%	0.2%	0.3%	***pb***
				2.4%	0.1%	0.0%	0.2%	0.2%	0.6%	***Dfd***
Fab-7[1]	***lab***	**2.4%**			**9.0%**	3.5%	0.9%	1.1%	3.1%	***scr***
	pb	0.1%	**0.6%**			**14.6%**	3.6%	1.5%	5.3%	***Antp***
	Dfd	0.3%	0.1%	**3.1%**			**16.0%**	2.3%	6.4%	***Ubx***
	scr	0.0%	0.1%	0.9%	**14.9%**			**21.2%**	20.2%	***abd-A***
	Antp	0.1%	0.0%	0.1%	6.9%	**18.5%**			**65.2%**	***Abd-B***
	Ubx	0.3%	0.1%	0.3%	1.8%	5.0%	**18.9%**			
	abd-A	0.0%	0.1%	0.3%	1.2%	2.0%	2.2%	**17.7%**		
	Abd-B	0.1%	0.3%	0.5%	4.3%	6.5%	6.6%	17.5%	**49.0%**	
		lab	***pb***	***Dfd***	***scr***	***Antp***	***Ubx***	***abd-A***	***Abd-B***	

Wing disc cells:

		WT								
		lab	***pb***	***Dfd***	***scr***	***Antp***	***Ubx***	***abd-A***	***Abd-B***	
		0.2%	0.0%	0.0%	0.0%	0.0%	0.0%	0.0%	0.0%	***lab***
			0.0%	0.0%	0.0%	0.0%	0.0%	0.0%	0.0%	***pb***
				0.6%	0.0%	0.0%	0.2%	0.0%	0.1%	***Dfd***
Fab-7[1]	***lab***	**0.7%**			**5.0%**	1.7%	2.9%	0.0%	0.2%	***scr***
	pb	0.0%	**0.0%**			**20.2%**	8.4%	0.2%	0.8%	***Antp***
	Dfd	0.4%	0.0%	**1.0%**			**59.8%**	0.5%	2.8%	***Ubx***
	scr	0.4%	0.0%	0.5%	**7.1%**			**0.8%**	0.5%	***abd-A***
	Antp	0.3%	0.0%	0.1%	2.9%	**25.1%**			**4.7%**	***Abd-B***
	Ubx	0.5%	0.0%	0.3%	3.1%	6.4%	**44.8%**			
	abd-A	0.0%	0.0%	0.0%	0.0%	0.5%	1.0%	**1.2%**		
	Abd-B	0.3%	0.0%	0.1%	1.0%	2.7%	5.2%	0.9%	**8.7%**	
		lab	***pb***	***Dfd***	***scr***	***Antp***	***Ubx***	***abd-A***	***Abd-B***	

Supplemental references

S1. Szabo, Q., Jost, D., Chang, J.M., Cattoni, D.I., Papadopoulos, G.L., Bonev, B., Sexton, T., Gurgo, J., Jacquier, C., Nollmann, M., et al. (2018). TADs are 3D structural units of higher-order chromosome organization in Drosophila. Sci Adv 4, eaar8082. 10.1126/sciadv.aar8082.